Effect of inhibitory spike-timing-dependent plasticity on fast sparsely synchronized rhythms in a small-world neuronal network

Sang-Yoon Kim, Woochang Lim *

Institute for Computational Neuroscience and Department of Science Education, Daegu National University of Education, Daegu 42411, Republic of Korea

HIGHLIGHTS

- An inhibitory small-world network of fast spiking interneurons is considered.
- Effects of inhibitory spike-timing-dependent plasticity are investigated.
- A "Matthew" effect in inhibitory synaptic plasticity is found to occur.
- Emergences of LTD and LTP are investigated via a microscopic studies.
- Effects of network architecture on FSS are studied in the presence of iSTDP.

ARTICLE INFO

ABSTRACT

We consider the Watts–Strogatz small-world network (SWN) consisting of inhibitory fast spiking Izhikevich interneurons. This inhibitory neuronal population has adaptive dynamic synaptic strengths governed by the inhibitory spike-timing-dependent plasticity (iSTDP). In previous works without iSTDP, fast sparsely synchronized rhythms, associated with diverse cognitive functions, were found to appear in a range of large noise intensities for fixed strong synaptic inhibition strengths. Here, we investigate the effect of iSTDP on fast sparse synchronization (FSS) by varying the noise intensity D. We employ an asymmetric anti-Hebbian time window for the iSTDP update rule [which is in contrast to the Hebbian time window for the excitatory STDP (eSTDP)]. Depending on values of D, population-averaged values of saturated synaptic inhibition strengths are potentiated [long-term potentiation (LTP)] or depressed [long-term depression (LTD)] in comparison with the initial mean value, and dispersions from the mean values of LTP/LTD are much increased when compared with the initial dispersion, independently of D. In most cases of LTD where the effect of mean LTD is dominant in comparison with the effect of dispersion, good synchronization (with higher spiking measure) is found to get better via LTD, while bad synchronization (with lower spiking measure) is found to get worse via LTP. This kind of Matthew effect in inhibitory synaptic plasticity is in contrast to that in excitatory synaptic plasticity where good (bad) synchronization gets better (worse) via LTP (LTD). Emergences of LTD and LTP of synaptic inhibition strengths are intensively investigated via a microscopic method based on the distributions of time delays between the pre- and the post-synaptic spike times. Furthermore, we also investigate the effects of network architecture on FSS by changing the rewiring probability p of the SWN in the presence of iSTDP.

© 2018 Published by Elsevier Ltd.

1. Introduction

In recent years, brain rhythms have attracted much attention (Buzsáki, 2006; Buzsáki & Wang, 2012; Garcia-Rill, 2015; Khodagholy, Gelinas, & Buzsáki, 2017; Michalareas et al., 2016; Miyawaki & Diba, 2016; Oliva, Fernández-Ruiz, Buzsáki, & Berényi, 2016; Ploner, Sorg, & Gross, 2017; Roux, Hu, Eichler, Stark, & Buzsáki, 2017; Saleem et al., 2017; Swann et al., 2017; Taxidis,

Anastassiou, Diva, & Koch, 2015; Traub & Whittington, 2010; Ujma et al., 2015; Veit, Hakim, Jadi, Sejnowski, & Adesnik, 2017). Particularly, we are interested in fast sparsely synchronized rhythms, associated with diverse cognitive functions (e.g., sensory perception, feature integration, selective attention, and memory formation) (Wang, 2010). At the population level, fast sparsely synchronous oscillations [e.g., gamma rhythm (30–100 Hz) during awake behaving states and rapid eye movement sleep and sharp-wave ripple (100–200 Hz) during quiet sleep and awake immobility] have been observed in local field potential recordings, while at the cellular level individual neuronal recordings have been found

---

to exhibit irregular and intermittent spike discharges like Geiger counters (Buhl, Tamas, & Fisahn, 1998; Csicsvari, Hirase, Czurko, & Buzsáki, 1998; Csicsvari, Hirase, Czurko, Mamiya, & Buzsáki, 1999; Fellous & Sejnowski, 2000; Fisahn, Pike, Buhl, & Paulsen, 1998; Fries, Reynolds, Rorie, & Desimone, 2001; Logothetis, Pauls, Augath, Trinath, & Oeltermann, 2001). Thus, single-cell firing activity differs distinctly from the population oscillatory behavior. We note that these fast sparsely synchronized rhythms are in contrast to fully synchronized rhythms where individual neurons fire regularly at the population frequency like clocks. Under the balance between strong external noise and strong recurrent inhibition, fast sparse synchronization (FSS) was found to appear in both random networks (Brunel, 2000; Brunel & Hakim, 1999; Brunel & Wang, 2003; Geisler, Brunel, & Wang, 2005) and globally-coupled networks (Brunel & Hakim, 2008; Brunel & Hansel, 2006). In brain networks, architecture of synaptic connections has been found to have complex topology (e.g., small-worldness and scale-freeness) which is neither regular nor completely random (Bassett & Bullmore, 2006; Bullmore & Sporns, 2009; Chklovskii, Mel, & Svoboda, 2004; Larimer & Strowbridge, 2008; Song, Sjöström, Reigl, Nelson, & Chklovskii, 2005; Sporns, 2011; Sporns & Honey, 2006; Sporns, Tononi, & Edelman, 2000). In our recent works (Kim & Lim, 2015a, b), as complex networks we employed the small-world network and the scale-free network, and studied the effects of network architecture on emergence of FSS.

In the previous works on FSS, synaptic coupling strengths were static. However, in real brains synaptic strengths may change to adapt to the environment [i.e., they can be potentiated (Hebb, 1949; Kornoski, 1948; Shatz, 1992) or depressed (Bienenstock, Cooper, & Munro, 1982; Sejnowski, 1977; Stent, 1973; von der Malsburg, 1973)]. These adjustments of synapses are called the synaptic plasticity which provides the basis for learning, memory, and development (Abbott & Nelson, 2000). Regarding the synaptic plasticity, we consider a spike-timing-dependent plasticity (STDP) (Bi & Poo, 2001; Caporale & Dan, 2008; Dan & Poo, 2004, 2006; Feldman, 2012; Kepecs, van Rossum, Song, & Tegner, 2002; Markram, Gerstner, & Sjöström, 2012; Song, Miller, & Abbott, 2000). For the STDP, the synaptic strengths vary via an update rule depending on the relative time difference between the pre- and the post-synaptic spike times. Many models for STDP have been employed to explain results on synaptic modifications occurring in diverse neuroscience topics for health and disease [e.g., temporal sequence learning (Abbott & Blum, 1996), temporal pattern recognition (Feldman, 2000), coincidence detection (Gerstner, Kempter, van Hemmen, & Wagner, 1996), navigation (Blum & Abbott, 1996), direction selectivity (Mehta & Wilson, 2000), memory consolidation (Ji & Wilson, 2007), competitive/selective development (Song & Abbott, 2001), and deep brain stimulation (Lourens, Schwab, Nirody, Meijer, & van Gils, 2015)]. Recently, the effects of STDP on population synchronization in ensembles of coupled neurons were also studied in various aspects (Borges et al., 2016; Borges, Borges, Lameu, Batista et al., 2017; Kim & Lim, 2018b, c; Popovych & Tass, 2012; Popovych, Yanchuk, & Tass, 2013).

A neural circuit in the brain cortex is composed of a few types of excitatory principal cells and diverse types of inhibitory interneurons. These interneurons make up about 20 percent of all cortical neurons, and exhibit diversity in their morphologies and functions (Buzsáki, Geisler, Henze, & Wang, 2004). By providing a synchronous oscillatory output to the principal cells, interneuronal networks play the role of backbones of many cortical rhythms (Buzsáki & Wang, 2012; Golomb & Rinzel, 1994; Wang, 2003; Wang & Buzsáki, 1996). Synaptic plasticity of excitatory and inhibitory connections is of great interest because it controls the efficacy of potential computational functions of excitation and inhibition. Studies of synaptic plasticity have been mainly focused on synaptic connections between excitatory pyramidal cells, because

excitatory-to-excitatory (E to E) connections are most prevalent in the cortex and they form a relatively homogeneous population (Bi & Poo, 1998; Debanne, Gähwiler, & Thompson, 1998; Egger, Feldmeyer, & Sakmann, 1999; Feldman, 2000; Gerstner et al., 1996; Markram, Lübke, Frotscher, & Sakmann, 1997; Tzounopoulos, Kim, Oertel, & Trussell, 2004; Wittenberg & Wang, 2006; Zhang, Tao, Holt, Harris, & Poo, 1998). An asymmetric Hebbian time window was employed for the excitatory STDP (eSTDP) update rule (Bi & Poo, 2001; Caporale & Dan, 2008; Dan & Poo, 2004, 2006; Feldman, 2012; Kepecs et al., 2002; Markram et al., 2012; Song et al., 2000). When a pre-synaptic spike precedes a post-synaptic spike, long-term potentiation (LTP) occurs; otherwise, long-term depression (LTD) appears. On the other hand, plasticity of inhibitory connections has attracted less attention mainly because of experimental obstacles and diversity of interneurons (Froemke, 2015; Gaiarsa, Caillard, & Ben-Ari, 2002; Kullmann, Moreau, Bakiri, & Nicholson, 2012; Lamsa, Kullmann, & Woodin, 2010; Vogels et al., 2013). With the advent of fluorescent labeling and optical manipulation of neurons according to their genetic types (Cardin, 2012; Deisseroth et al., 2006), inhibitory plasticity has also begun to be focused. Particularly, studies on iSTDP of inhibitory-to-excitatory (I to E) connections have been much made. Thus, inhibitory STDP (iSTDP) has been found to be diverse and cell-specific (Borges, Borges, Lameu, Protachevicz et al., 2017; Castilo, Chiu, & Carroll, 2011; Froemke, 2015; Gaiarsa et al., 2002; Haas, Nowotny, & Abarbanel, 2006; Kullmann et al., 2012; Lamsa et al., 2010; Soto-Trevino, Thoroughman, Marder, & Abbott, 2001; Talathi, Hwang, & Ditto, 2008; Vogels et al., 2013; Vogels, Sprekeler, Zenke, Clopath, & Gerstner, 2011; Woodin, Ganguly, & Poo, 2003).

In this paper, we consider an inhibitory Watts–Strogatz small-world network (SWN) of fast spiking (FS) interneurons (Strogatz, 2001; Watts, 2003; Watts & Strogatz, 1998), and investigate the effect of iSTDP [of inhibitory-to-inhibitory (I to I) connections] on FSS by varying the noise intensity D. We employ an asymmetric anti-Hebbian time window for the iSTDP update rule, in contrast to the Hebbian time window for the eSTDP (Lourens et al., 2015; Popovych & Tass, 2012). Then, strengths of synaptic inhibition $\{J_{ij}\}$ change with time, and eventually, they become saturated after a sufficiently long time. Depending on D, mean values of saturated synaptic inhibition strengths $\{J_{ij}^*\}$ are potentiated [long-term potentiation (LTP)] or depressed [long-term depression (LTD)], when compared with the initial mean value of synaptic inhibition strengths. On the other hand, dispersions from the mean values of LTP/LTD are much increased in comparison with the initial dispersion, irrespectively of D.

For the case of iSTDP, both the mean value and the dispersion (for the distribution of synaptic inhibition strengths) affect population synchronization. The LTD (LTP) tends to increase (decrease) the degree of FSS due to decrease (increase) in the mean value of synaptic inhibition strengths, and the increased dispersions decrease the degree of FSS. For most cases of LTD where the effect of mean LTD is dominant in comparison with the effect of dispersion, good synchronization (with higher spiking measure) gets better via LTD; in some other cases where dispersions are dominant, the degree of good synchronization may be decreased even in the case of LTD. On the other hand, in all cases bad synchronization (with lower spiking measure) gets worse via LTP. This kind of Matthew effect (valid in most cases of LTD) is in contrast to that in the case of eSTDP where good (bad) synchronization gets better (worse) via LTP (LTD) (Kim & Lim, 2018b, c); the role of LTD (LTP) in the case of iSTDP is similar to that of LTP (LTD) for the case of eSTDP. Emergences of LTD and LTP of synaptic inhibition strengths are also investigated through a microscopic method based on the distributions of time delays between the nearest spiking times of the pre- and the post-synaptic interneurons. Moreover, we study the effects of network architecture on FSS by varying the rewiring probability p of the SWN in the presence of iSTDP.

This paper is organized as follows. In Section 2, we describe an inhibitory Watts–Strogatz SWN of FS interneurons with inhibitory synaptic plasticity. Then, in Section 3 the effects of iSTDP on FSS are investigated. Finally, we give summary and discussion in Section 4.

2. Watts–Strogatz SWN of FS Izhikevich interneurons with inhibitory synaptic plasticity

We consider an inhibitory directed Watts–Strogatz SWN, composed of N FS interneurons equidistantly placed on a one-dimensional ring of radius $N/2\pi$. The Watts–Strogatz SWN interpolates between a regular lattice with high clustering (corresponding to the case of $p = 0$) and a random graph with short average path length (corresponding to the case of $p = 1$) via random uniform rewiring with the probability p (Strogatz, 2001; Watts, 2003; Watts & Strogatz, 1998). For $p = 0$, we start with a directed regular ring lattice with N nodes where each node is coupled to its first M_{syn} neighbors ($M_{syn}/2$ on either side) via outward synapses, and rewire each outward connection uniformly at random over the whole ring with the probability p (without self-connections and duplicate connections). This Watts–Strogatz SWN model may be regarded as a cluster-friendly extension of the random network by reconciling the six degrees of separation (small-worldness) (Guare, 1990; Milgram, 1967) with the circle of friends (clustering). These SWNs with predominantly local connections and rare long-range connections were employed in many recent works on various subjects of neurodynamics (Achard & Bullmore, 2007; Kaiser & Hilgetag, 2006; Kwon & Moon, 2002; Lago-Fernández, Huerta, Corbacho, & Sigüenza, 2000; Lizier, Pritam, & Prokopenko, 2011; Ozer, Perc, & Uzuntarla, 2009; Riecke, Roxin, Madruga, & Solla, 2007; Roxin, Riecke, & Solla, 2004; Shanahan, 2008; Wang, Duan, Perc, & Chen, 2008; Wang, Perc, Duan, & Chen, 2010; Yu, Huang, Singer, & Nikolie, 2008).

As elements in our SWN, we choose the Izhikevich inhibitory FS interneuron model which is not only biologically plausible, but also computationally efficient (Izhikevich, 2003, 2004, 2007, 2010). Unlike Hodgkin–Huxley-type conductance-based models, the Izhikevich model matches neuronal dynamics by tuning the parameters instead of matching neuronal electrophysiology. The parameters k and b are associated with the neuron's rheobase and input resistance, and a, c, and d are the recovery time constant, the after-spike reset value of v, and the after-spike jump value of u, respectively. Tuning these parameters, the Izhikevich neuron model may produce 20 of the most prominent neuro-computational features of biological neurons (Izhikevich, 2003, 2004, 2007, 2010). Particularly, the Izhikevich model is used to reproduce the six most fundamental classes of firing patterns observed in the mammalian neocortex; (a) excitatory regular spiking pyramidal neurons, (b) inhibitory FS interneurons, (c) intrinsic bursting neurons, (d) chattering neurons, (e) low-threshold spiking neurons and (f) late spiking neurons (Izhikevich, 2007). Here, we use the parameter values for the FS interneurons (which do not fire postinhibitory rebound spikes) in the layer 5 rat visual cortex, which are listed in the 1st item of Table 1 [see the caption of Fig. 8.27 in Izhikevich (2007)].

The following Eqs. (1)–(6) govern the population dynamics in the SWN:

$$C\frac{dv_i}{dt} = k(v_i - v_r)(v_i - v_t) - u_i + I_i + D\xi_i - I_{syn,i}, \quad (1)$$

$$\frac{du_i}{dt} = a\{U(v_i) - u_i\}, \quad i = 1, \ldots, N, \quad (2)$$

with the auxiliary after-spike resetting:

if $v_i \geq v_p$, then $v_i \leftarrow c$ and $u_i \leftarrow u_i + d$, (3)

Table 1
Parameter values used in our computations; units of the capacitance, the potential, the current, and the time are pF, mV, pA, and ms, respectively.

(1)	Single Izhikevich fast spiking interneurons (Izhikevich, 2007)			
	$C = 20$	$v_r = -55$	$v_t = -40$	$v_p = 25$	$v_b = -55$
	$k = 1$	$a = 0.2$	$b = 0.025$	$c = -45$	$d = 0$
(2)	Random external excitatory input to each Izhikevich fast spiking Interneurons			
	$I_i \in [680, 720]$		D: Varying	
(3)	Inhibitory synapse mediated by the GABA$_A$ neurotransmitter (Brunel & Wang, 2003)			
	$\tau_l = 1$	$\tau_r = 0.5$	$\tau_d = 5$	$V_{syn} = -80$
(4)	Synaptic connections between interneurons in the Watts–Strogatz SWN			
	$M_{syn} = 50$	p: Varying		
	$J_0 = 700$	$\sigma_0 = 5$	$J_{ij} \in [0.0001, 2000]$	
(5)	Anti-Hebbian iSTDP rule			
	$\delta = 0.05$	$A_+ = 1.0$	$A_- = 1.1$	$\tau_+ = 11.5$	$\tau_- = 12$

where

$$U(v) = \begin{cases} 0 & \text{for } v < v_b \\ b(v - v_b)^3 & \text{for } v \geq v_b \end{cases}, \quad (4)$$

$$I_{syn,i} = \frac{1}{d_i^{(in)}} \sum_{j=1(j\neq i)}^{N} J_{ij} w_{ij} s_j(t)(v_i - V_{syn}), \quad (5)$$
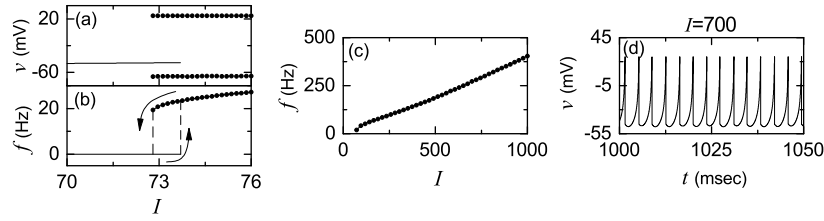
$$s_j(t) = \sum_{f=1}^{F_j} E(t - t_f^{(j)} - \tau_l); \; E(t)$$

$$= \frac{1}{\tau_d - \tau_r}(e^{-t/\tau_d} - e^{-t/\tau_r})\Theta(t). \quad (6)$$

Here, the state of the ith neuron at a time t is characterized by two state variables: the membrane potential v_i and the recovery current u_i. In Eq. (1), C is the membrane capacitance, v_r is the resting membrane potential, and v_t is the instantaneous threshold potential. After the potential reaches its apex (i.e., spike cutoff value) v_p, the membrane potential and the recovery variable are reset according to Eq. (3). The units of the capacitance C, the potential v, the current u and the time t are pF, mV, pA, and ms, respectively. The parameter values used in our computations are listed in Table 1. More details on the random external excitatory input to each Izhikevich FS interneuron, the synaptic currents and plasticity, and the numerical method for integration of the governing equations are given in the following subsections.

2.1. Random external excitatory input to each Izhikevich FS interneuron

Each interneuron in the network receives stochastic external excitatory input $I_{ext,i}$ from other brain regions, not included in the network (i.e., corresponding to background excitatory input) (Brunel, 2000; Brunel & Hakim, 1999; Brunel & Wang, 2003; Geisler et al., 2005; Golomb & Rinzel, 1994). Then, $I_{ext,i}$ may be modeled in terms of its time-averaged constant I_i and an independent Gaussian white noise ξ_i (i.e., corresponding to fluctuation of $I_{ext,i}$ from its mean) [see the 3rd and the 4th terms in Eq. (1)] satisfying $\langle \xi_i(t) \rangle = 0$ and $\langle \xi_i(t) \xi_j(t') \rangle = \delta_{ij} \delta(t - t')$, where $\langle \cdots \rangle$ denotes the ensemble average. The intensity of the noise ξ_i is controlled by using the parameter D. In the absence of noise (i.e., $D = 0$), the Izhikevich interneuron exhibits a jump from a resting state to a spiking state via subcritical Hopf bifurcation for $I_h = 73.7$ by absorbing an unstable limit cycle born via a fold limit cycle bifurcation for $I_l = 72.8$, as shown in Fig. 1(a) (Kim & Lim, 2015a). Hence, the Izhikevich FS interneuron shows type-II excitability because it begins to fire with a non-zero frequency [see Fig. 1(b)] (Hodgkin, 1948; Izhikevich, 2000). As I is increased from I_h, the mean firing rate (MFR) f

Fig. 1. Single FS Izhikevich interneuron for $D = 0$. (a) Bifurcation diagram. Solid line denotes a stable equilibrium point, and maximum and minimum values of v for the spiking state are represented by solid circles. Plot of the mean firing rate f versus the time-averaged constant I of the random external excitatory input (b) near the transition point and (c) in a large range of I. (d) Time series of the membrane potential v for $I = 700$.

increases monotonically, as shown in Fig. 1(c). Throughout this paper, we consider a suprathreshold case such that the value of I_i is chosen via uniform random sampling in the range of [680,720], as shown in the 2nd item of Table 1; for the middle value of $I = 700$, the membrane potential v oscillates very fast with $f = 271$ Hz [see Fig. 1(d)].

2.2. Synaptic currents and plasticity

The last term in Eq. (1) represents the synaptic couplings of Izhikevich FS interneurons. $I_{syn,i}$ of Eq. (5) represents a synaptic current injected into the ith interneuron, and V_{syn} is the synaptic reversal potential. The synaptic connectivity is given by the connection weight matrix $W (= \{w_{ij}\})$ where $w_{ij} = 1$ if the interneuron j is presynaptic to the interneuron i; otherwise, $w_{ij} = 0$. Here, the synaptic connection is modeled in terms of the Watts–Strogatz SWN. Then, the in-degree of the ith neuron, $d_i^{(in)}$ (i.e., the number of synaptic inputs to the interneuron i) is given by $d_i^{(in)} = \sum_{j=1(j \neq i)}^{N} w_{ij}$. For this case, the average number of synaptic inputs per neuron is given by $M_{syn} = \frac{1}{N} \sum_{i=1}^{N} d_i^{(in)}$. Throughout the paper, $M_{syn} = 50$ (see the 4th item of Table 1). The fraction of open synaptic ion channels at time t is denoted by $s(t)$. The time course of $s_j(t)$ of the jth neuron is given by a sum of delayed double-exponential functions $E(t - t_f^{(j)} - \tau_l)$ [see Eq. (6)], where τ_l is the synaptic delay, and $t_f^{(j)}$ and F_j are the fth spike and the total number of spikes of the jth interneuron at time t, respectively. Here, $E(t)$ [which corresponds to contribution of a presynaptic spike occurring at time 0 to $s_j(t)$ in the absence of synaptic delay] is controlled by the two synaptic time constants: synaptic rise time τ_r and decay time τ_d, and $\Theta(t)$ is the Heaviside step function: $\Theta(t) = 1$ for $t \geq 0$ and 0 for $t < 0$. For the inhibitory GABAergic synapse (involving the GABA$_A$ receptors), the values of τ_l, τ_r, τ_d, and V_{syn} are listed in the 3rd item of Table 1 (Brunel & Wang, 2003).

The coupling strength of the synapse from the jth pre-synaptic interneuron to the ith post-synaptic interneuron is J_{ij}. Here, we consider a multiplicative iSTDP (dependent on states) for the synaptic strengths $\{J_{ij}\}$ (Popovych et al., 2013; Rubin, Lee, & Sompolinsky, 2001). To avoid unbounded growth and elimination of synaptic connections, we set a range with the upper and the lower bounds: $J_{ij} \in [J_l, J_h]$, where $J_l = 0.0001$ and $J_h = 2000$. Initial synaptic strengths are normally distributed with the mean $J_0(= 700)$ and the standard deviation $\sigma_0(= 5)$. With increasing time t, the synaptic strength for each synapse is updated with a nearest-spike pair-based STDP rule (Morrison, Aertsen, & Diesmann, 2007):

$$J_{ij} \rightarrow J_{ij} + \delta(J^* - J_{ij}) |\Delta J_{ij}(\Delta t_{ij})|, \tag{7}$$

where $\delta (= 0.05)$ is the update rate, $J^* = J_h (J_l)$ for the LTP (LTD), and $\Delta J_{ij}(\Delta t_{ij})$ is the synaptic modification depending on the relative time difference $\Delta t_{ij} (= t_i^{(post)} - t_j^{(pre)})$ between the nearest spike times of the post-synaptic interneuron i and the presynaptic interneuron j. We use an asymmetric anti-Hebbian time

window for the synaptic modification $\Delta J_{ij}(\Delta t_{ij})$ (Lourens et al., 2015; Popovych & Tass, 2012):

$$\Delta J_{ij}(\Delta t_{ij}) = \begin{cases} -A_+ \, e^{-\Delta t_{ij}/\tau_+} & \text{for } \Delta t_{ij} > 0 \\ -A_- \dfrac{\Delta t_{ij}}{\tau_-} e^{\Delta t_{ij}/\tau_-} & \text{for } \Delta t_{ij} \leq 0 \end{cases}, \tag{8}$$

where $A_+ = 1.0$, $A_- = 1.1$, $\tau_+ = 11.5$ ms, and $\tau_- = 12$ ms (these values are also given in the 5th item of Table 1). For the case of $\Delta t_{ij} > 0$, LTD occurs, while LTP takes place in the case of $\Delta t_{ij} < 0$, in contrast to the Hebbian time window for the eSTDP where LTP (LTD) occurs for $\Delta t_{ij} > (<)0$ (Kim & Lim, 2018c).

2.3. Numerical method for integration

Numerical integration of stochastic differential Eqs. (1)–(6) with an anti-Hebbian iSTDP rule of Eqs. (7) and (8) is done by employing the Heun method (San Miguel & Toral, 2000) with the time step $\Delta t = 0.01$ ms. For each realization of the stochastic process, we choose random initial points $[v_i(0), u_i(0)]$ for the ith $(i = 1, \ldots, N)$ FS interneuron with uniform probability in the range of $v_i(0) \in (-50, -45)$ and $u_i(0) \in (10, 15)$.

3. Effect of inhibitory STDP on fast sparsely synchronized rhythms

We consider the Watts–Strogatz SWN with high clustering and short path length when the rewiring probability p is 0.25. This SWN is composed of N inhibitory Izhikevich FS interneurons. Throughout the paper, $N = 10^3$ except for the cases in Fig. 2(a) and in Fig. 4(b1), (b2), and (c).

3.1. FSS in the absence of iSTDP

First, we are concerned about FSS in the absence of iSTDP in the SWN with $p = 0.25$. The coupling strengths $\{J_{ij}\}$ are static, and their values are chosen from the Gaussian distribution with the mean $J_0 (= 700)$ and the standard deviation $\sigma_0 (=5)$. Population synchronization may be well visualized in the raster plot of neural spikes which is a collection of spike trains of individual interneurons. Such raster plots of spikes are fundamental data in experimental neuroscience. As a collective quantity showing population behaviors, we use an instantaneous population spike rate (IPSR) which may be obtained from the raster plots of spikes (Brunel, 2000; Brunel & Hakim, 1999, 2008; Brunel & Hansel, 2006; Brunel & Wang, 2003; Geisler et al., 2005; Kim & Lim, 2014; Wang, 2010). For the synchronous case, "stripes" (composed of spikes and indicating population synchronization) are found to be formed in the raster plot, while in the desynchronized case spikes are completely scattered. Hence, for a synchronous case, an oscillating IPSR $R(t)$ appears, while for a desynchronized case $R(t)$ is nearly stationary. To obtain a smooth IPSR, we employ the kernel density estimation (kernel smoother) (Shimazaki & Shinomoto, 2010).

Each spike in the raster plot is convoluted (or blurred) with a kernel function $K_h(t)$ to obtain a smooth estimate of IPSR $R(t)$:

$$R(t) = \frac{1}{N} \sum_{i=1}^{N} \sum_{s=1}^{n_i} K_h(t - t_s^{(i)}), \tag{9}$$

where $t_s^{(i)}$ is the sth spiking time of the ith interneuron, n_i is the total number of spikes for the ith neuron, and we use a Gaussian kernel function of band width h:

$$K_h(t) = \frac{1}{\sqrt{2\pi}h} e^{-t^2/2h^2}, \quad -\infty < t < \infty. \tag{10}$$

Throughout the paper, the band width h of $K_h(t)$ is 1 ms.

The mean square deviation of $R(t)$,

$$\mathcal{O} \equiv \overline{(R(t) - \overline{R(t)})^2}, \tag{11}$$

plays the role of an order parameter $\mathcal{O}$ (Kim & Lim, 2014); the overbar represents the time average. This order parameter may be regarded as a thermodynamic measure because it concerns just the macroscopic IPSR kernel estimate $R(t)$ without any consideration between $R(t)$ and microscopic individual spikes. In the thermodynamic limit of $N \to \infty$, the order parameter $\mathcal{O}$ approaches a non-zero (zero) limit value for the synchronized (desynchronized) state. Fig. 2(a) shows plots of $\log_{10}\langle \mathcal{O} \rangle_r$ versus D. In each realization, we discard the first time steps of a stochastic trajectory as transients for 10^3 ms, and then we numerically compute $\mathcal{O}$ by following the stochastic trajectory for 3×10^4 ms. Throughout the paper, $\langle \cdots \rangle_r$ denotes an average over 20 realizations. With increasing N up to 10^4, these numerical calculations for $\langle \mathcal{O} \rangle_r$ are done for various values of D. For $D < D^*(\simeq 558)$, synchronized states exist because the order parameter $\langle \mathcal{O} \rangle_r$ tends to converge toward non-zero limit values. On the other hand, for $D > D^*$, with increasing N the order parameter $\langle \mathcal{O} \rangle_r$ tends to approach zero, and hence a transition to desynchronization occurs due to a destructive role of noise spoiling the population synchronization.

Fig. 2(b1)–(b6) show raster plots of spikes for various values of D, and their corresponding IPSR kernel estimates $R(t)$ are also shown in Fig. 2(c1)–(c6). For $D = 50$, clear (straight) stripes appear successively in the raster plot of spikes, as shown in Fig. 2(b1), and the corresponding IPSR $R(t)$ exhibits a regular oscillation [see Fig. 2(c1)]. However, as D is increased, the raster plot of spikes begins to show a zigzag pattern intermingled with inclined partial stripes of spikes due to local clustering, as shown in Fig. 2(b2) for $D = 150$, and hence the amplitudes of the IPSR $R(t)$ are reduced so much in comparison with those for $D = 50$ [see Fig. 2(c2)]. With further increase in D, zigzag stripes in the raster plot are smeared (see the cases of $D = 250$, 350, and 450), and hence the amplitudes of $R(t)$ decrease. Eventually, when passing D^* desynchronization occurs due to overlap of smeared zigzag stripes, as shown in Fig. 2(b6) for $D = 750$, and then the IPSR $R(t)$ becomes nearly stationary (i.e., no population rhythm appears) [see Fig. 2(c6)].

In the synchronized region for $D < D^*$, we also compare population oscillating behaviors of $R(t)$ with spiking behaviors of individual interneurons. Fig. 2(d) shows plots of the population frequency $\langle f_p \rangle_r$ (represented by open circles) and the population-averaged MFR $\langle \langle f_i \rangle \rangle_r$ (denoted by crosses) of individual interneurons versus D. In each realization, we get f_p from the one-sided power spectrum of $\Delta R(t) (= R(t) - \overline{R(t)})$ (the overbar represents the time average) with mean-squared amplitude normalization which is obtained from 2^{16} data points, and also obtain the MFR f_i for each interneuron through averaging for 2×10^4 ms; $\langle \cdots \rangle$ denotes a population average over all interneurons. As examples, power spectra are shown for various values of D in Fig. 2(e1)–(e5). Moreover, interspike interval (ISI) histograms for individual interneurons are also given in Fig. 2(f1)–(f6). For each D, we obtain the ISI histogram via collecting 10^5 ISIs from all interneurons; the
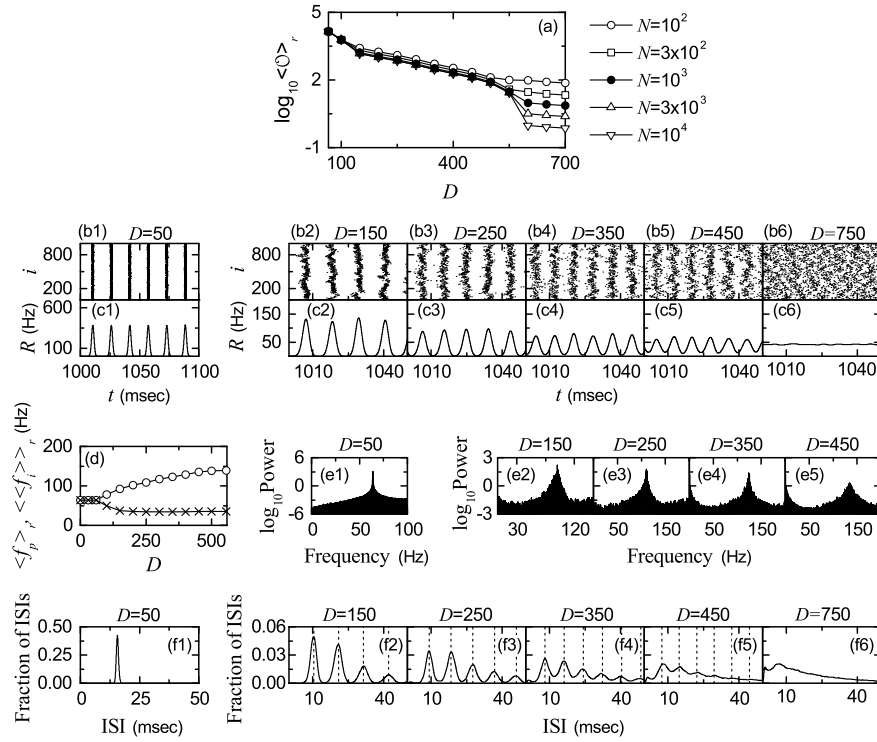
bin size for the histogram is 0.5 ms. For $D = 50$, $R(t)$ shows a regular oscillation with population frequency $\langle f_p \rangle_r \simeq 63.8$ Hz [see Fig. 2(e1)]. The ISI histogram in Fig. 2(f1) has a single peak, and $\langle ISI \rangle_r$ (average ISI) $\simeq 15.7$ ms. Hence, individual interneurons fire regularly like clocks with the population-averaged MFR $\langle \langle f_i \rangle \rangle_r$ which is the same as $\langle f_p \rangle_r$. For this case, all interneurons make firings in each spiking stripe in the raster plot (i.e., each stripe is fully occupied by spikes of all interneurons). Consequently, full synchronization with $\langle f_p \rangle_r = \langle \langle f_i \rangle \rangle_r$ occurs for $D = 50$. This kind of full synchronization persists until $D = D_{th} \simeq 65$, as shown in Fig. 2(d). However, when passing the threshold D_{th}, full synchronization is developed into sparse synchronization with $\langle f_p \rangle_r > \langle \langle f_i \rangle \rangle_r$ via a pitchfork bifurcation [see Fig. 2(d)].

For the case of sparse synchronization, individual interneurons fire at lower rates than the population frequency, and hence only a smaller fraction of interneurons fire in each spiking stripe in the raster plot (i.e., each stripe is sparsely occupied by spikes of a smaller fraction of interneurons). As D is increased, the occupation degree of spikes (representing the density of spiking stripes in the raster plot) decreases, along with decrease in the pacing degree of spikes (denoting smearing of spiking stripes), which results in decrease in amplitudes of $R(t)$ [see Fig. 2(c2)–(c5)]. We note that, with increasing D from D_{th}, the interval between stripes in the raster plot becomes smaller. Hence, the population frequency $\langle f_p \rangle_r$ increases monotonically, as shown in Fig. 2(d) [see also Fig. 2(e2)–(e5)]. As a result, fast sparsely synchronized rhythms appear in the range of $D_{th} < D < D^*$. On the other hand, the population-averaged MFR $\langle \langle f_i \rangle \rangle_r$ is much less than $\langle f_p \rangle_r$ due to sparse occupation of spikes in stripes [see Fig. 2(d)]. As a result, spiking behaviors of individual interneurons differs markedly from the fast population oscillatory behaviors.

Hereafter, we pay our attention to FSS (occurring for $D_{th} < D < D^*$). Unlike the case of full synchronization, individual interneurons exhibit intermittent spikings phase-locked to the IPSR $R(t)$ at random multiples of the global period T_G of $R(t)$. This "stochastic phase locking", leading to "stochastic spike skipping", is well shown in the ISI histogram with multiple peaks appearing at multiples of T_G, as shown in Fig. 2(f2)–(f5), in contrast to the case of full synchronization with a single-peaked ISI histogram. Similar skipping phenomena of spikings (characterized with multi-peaked ISI histograms) have also been found in networks of coupled inhibitory neurons in the presence of noise where noise-induced hopping from one cluster to another one occurs (Golomb & Rinzel, 1994), in single noisy neuron models exhibiting stochastic resonance due to a weak periodic external force (Longtin, 1995, 2000), and in inhibitory networks of coupled subthreshold neurons showing stochastic spiking coherence (Hong, Kim, & Lim, 2011; Kim & Lim, 2013; Lim & Kim, 2011). Due to this stochastic spike skipping, sparse occupation occurs in spiking stripes in the raster plot. For this case, the ensemble-averaged MFR $\langle \langle f_i \rangle \rangle_r$ of individual interneurons becomes less than the population frequency $\langle f_p \rangle_r$, which results in occurrence of sparse synchronization. We also note that, with increasing D, multiple peaks in the ISI histogram begin to merge [see Fig. 2(f2)–(f5)], and hence spiking stripes in the raster plot become more and more smeared (i.e., pacing degree of spikes in the raster plot decreases). Eventually, in the case of desynchronized states for $D > D^*$, multiple peaks overlap completely [e.g., see Fig. 2(f6) for $D = 750$], and hence spikes in the raster plot are completely scattered.

We now measure the degree of FSS in the range of $D_{th} < D < D^*$ by employing the statistical–mechanical spiking measure M_s (Kim & Lim, 2014). For the case of FSS, sparse stripes appear successively in the raster plot of spikes. The spiking measure M_i of the ith stripe is defined by the product of the occupation degree O_i of spikes (representing the density of the ith stripe) and the pacing degree P_i of spikes (denoting the smearing of the ith stripe):

$$M_i = O_i \cdot P_i. \tag{12}$$

Fig. 2. Population states in the absence of iSTDP. (a) Plots of the thermodynamic order parameter $\langle \mathcal{O} \rangle_r$ versus D. Raster plots of spikes in (b1)–(b6) and IPSR kernel estimates $R(t)$ in (c1)–(c6). (d) Plots of the population frequency $\langle f_p \rangle_r$ (represented by open circles) and the population-averaged MFR of individual interneurons $\langle \langle f_i \rangle \rangle_r$ (denoted by crosses) versus D. (e1)–(e5) Power spectra of $\Delta R(t)(= R(t) - \overline{R(t)})$ (the overbar represents the time average). ISI histograms in (f1)–(f6); vertical dotted lines represent multiples of the global period T_G of the IPSR $R(t)$.
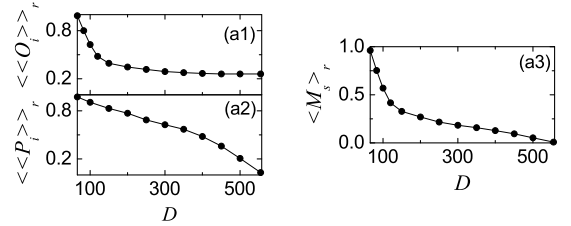
The occupation degree O_i of spikes in the stripe is given by the fraction of spiking neurons:

$$O_i = \frac{N_i^{(s)}}{N}, \tag{13}$$

where $N_i^{(s)}$ is the number of spiking neurons in the ith stripe. For the case of sparse synchronization, $O_i < 1$, in contrast to the case of full synchronization with $O_i = 1$. The pacing degree P_i of spikes in the ith stripe can be determined in a statistical–mechanical way by taking into account their contributions to the macroscopic IPSR $R(t)$. Central maxima of $R(t)$ between neighboring left and right minima of $R(t)$ coincide with centers of stripes in the raster plot. A global cycle begins from a left minimum of $R(t)$, passes a maximum, and ends at a right minimum. An instantaneous global phase $\Phi(t)$ of $R(t)$ was introduced via linear interpolation in the region forming a global cycle [for details, refer to Eqs. (16) and (17) in Kim and Lim (2014)]. Then, the contribution of the kth microscopic spike in the ith stripe occurring at the time $t_k^{(s)}$ to $R(t)$ is given by $\cos \Phi_k$, where Φ_k is the global phase at the kth spiking time [i.e., $\Phi_k \equiv \Phi(t_k^{(s)})$]. A microscopic spike makes the most constructive (in-phase) contribution to $R(t)$ when the corresponding global phase Φ_k is $2\pi n$ ($n = 0, 1, 2, \dots$). On the other hand, it makes the most destructive (anti-phase) contribution to $R(t)$ when Φ_k is $2\pi(n - 1/2)$. By averaging the contributions of all microscopic spikes in the ith stripe to $R(t)$, we get the pacing degree of spikes in the ith stripe [see Eq. (18) in Kim and Lim (2014)]:

$$P_i = \frac{1}{S_i} \sum_{k=1}^{S_i} \cos \Phi_k, \tag{14}$$

where S_i is the total number of microscopic spikes in the ith stripe. Then, through averaging M_i of Eq. (12) over a sufficiently large number N_s of stripes, we get the realistic statistical–mechanical

spiking measure M_s, based on the IPSR $R(t)$ [see Eq. (19) in Kim and Lim (2014)]:

$$M_s = \frac{1}{N_s} \sum_{i=1}^{N_s} M_i. \tag{15}$$

In each realization, we obtain M_s by following 3×10^3 stripes.

Fig. 3(a1)–(a3) show the average occupation degree $\langle \langle O_i \rangle \rangle_r$, the average pacing degree $\langle \langle P_i \rangle \rangle_r$, and the statistical–mechanical spiking measure $\langle M_s \rangle_r$, respectively. With increasing D from D_{th}, at first $\langle \langle O_i \rangle \rangle_r$ (denoting the density of stripes in the raster plot) decreases rapidly due to stochastic spike skipping, like the behavior of $\langle \langle f_i \rangle \rangle_r$ in Fig. 2(d), and then it tends to approach a limit value ($\simeq 0.26$). The average pacing degree $\langle \langle P_i \rangle \rangle_r$ represents well the smearing degree of stripes in the raster plot [shown in Fig. 2(b2)–(b5)]. With increasing D, $\langle \langle P_i \rangle \rangle_r$ decreases, and for large D near D^* it converges to zero rapidly due to complete overlap of sparse spiking stripes. Through product of the occupation and the pacing degrees of spikes, the statistical–mechanical spiking measure $\langle M_s \rangle_r$ is obtained. Due to the rapid decrease in $\langle \langle O_i \rangle \rangle_r$, at first $\langle M_s \rangle_r$ also

Fig. 3. Characterization of FSS in the absence of iSTDP. Plots of (a1) the average occupation degree $\langle \langle O_i \rangle \rangle_r$, (a2) the average pacing degree $\langle \langle P_i \rangle \rangle_r$, and (a3) the statistical–mechanical spiking measure $\langle M_s \rangle_r$ versus D.
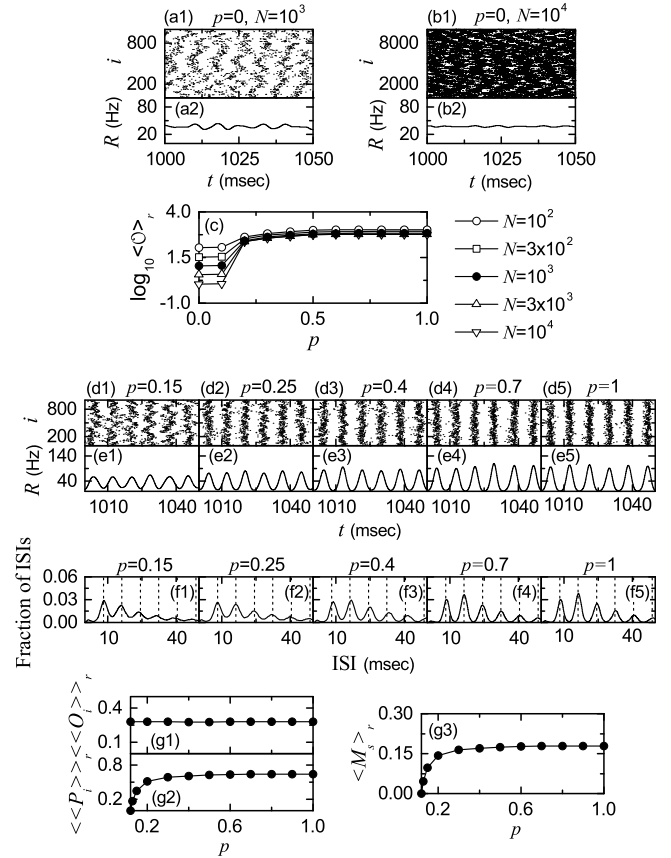
decreases rapidly, and then it makes a slow convergence to zero for $D = D^*$.

So far, we considered the case of $p = 0.25$. From now on, we fix the value of D at $D = 350$, and investigate the effect of small-world connectivity on FSS by varying the rewiring probability p. The topological properties of the small-world connectivity has been well characterized in terms of the clustering coefficient and the average path length (Watts & Strogatz, 1998). The clustering coefficient C, representing the cliquishness of a typical neighborhood in the network, characterizes the local efficiency of information transfer. On the other hand, the average path length L, denoting the typical separation between two nodes in the network, characterizes the global efficiency of information transfer. The Watts–Strogatz SWN interpolates between a regular lattice (corresponding to the case of $p = 0$) and a random graph (corresponding to the case of $p = 1$) through random uniform rewiring with the probability p (Watts & Strogatz, 1998). The regular lattice for $p = 0$ is highly clustered but large world where L grows linearly with N; $C \simeq 0.71$ and $L \simeq 17.5$ for $N = 10^3$ (Watts & Strogatz, 1998). On the other hand, the random graph for $p = 1$ is poorly clustered but small world where L grows logarithmically with N; $C \simeq 0.02$ and $L \simeq 2.64$ for $N = 10^3$ (Watts & Strogatz, 1998). As soon as p increases from zero, L decreases dramatically, which results in occurrence of a small-world phenomenon which is popularized by the phrase of the "six degrees of separation" (Guare, 1990; Milgram, 1967). However, during this dramatic drop in L, C decreases only a little. Consequently, for small p SWNs with short path length and high clustering appear (e.g., for $p = 0.25$, $C \simeq 0.33$ and $L \simeq 2.83$) (Watts & Strogatz, 1998).

We first consider the population state in the regular lattice for $p = 0$. As shown in Fig. 4(a1) for $N = 10^3$, the raster plot shows a zigzag pattern intermingled with inclined partial stripes of spikes, and $R(t)$ is composed of coherent parts with regular large-amplitude oscillations and incoherent parts with irregular small-amplitude fluctuations [see Fig. 4(a2)]. For $p = 0$, the clustering coefficient is high, and hence inclined partial stripes (indicating local clustering of spikes) seem to appear in the raster plot of spikes. As N is increased to 10^4, partial stripes become more inclined from the vertical [see Fig. 4(b1)], and hence spikes become more difficult to keep pace with each other. Consequently, $R(t)$ shows noisy fluctuations with smaller amplitudes, as shown in Fig. 4(b2). Hence, the population state for $p = 0$ seems to be desynchronized because $R(t)$ tends to be nearly stationary as N increases to the infinity. With increasing p from 0, long-range short-cuts begin to appear, and hence the average path length L becomes shorter. Hence, when global communication between distant neurons are sufficiently efficient, fast sparsely synchronized states may emerge. To examine appearance of FSS, we obtain the order parameter $\mathcal{O}$ of Eq. (11) by varying p. Fig. 4(c) shows plots of the order parameter $\langle \mathcal{O} \rangle_r$ versus p. For $p < p^* (\simeq 0.12)$, desynchronized states exist because $\langle \mathcal{O} \rangle_r$ tends to zero as N is increased. However, when passing the critical value p^*, a transition to FSS occurs because the values of $\langle \mathcal{O} \rangle_r$ become saturated to nonzero limit values.

We now study population and individual behaviors of FSS for $p > p^*$. FSS can be understood well via comparison of population behaviors with individual behaviors. Fig. 4(d1)–(d5) and (e1)–(e5) show raster plots of spikes and IPSR kernel estimates $R(t)$ for various values of p, respectively. As p is increased, the zigzagness degree of partial stripes in the raster plots becomes reduced due to decrease in the clustering coefficient [see Fig. 4(d1)–(d5)]. For $p = \tilde{p} (\sim 0.7)$, the raster plot becomes composed of vertical stripes without zigzag, and then the pacing degree between spikes for $p > \tilde{p}$ becomes nearly the same. As a result, the amplitudes of $R(t)$ increase until $p = \tilde{p}$, and then they become nearly saturated. For all these values of p, $R(t)$ exhibit regular oscillations with the same

Fig. 4. Effect of network architecture on FSS for $D = 350$ in the absence of iSTDP. Desynchronized state for $p = 0$: raster plots of spikes in (a1) and (b1) and IPSR kernel estimates $R(t)$ in (a2) and (b2) for $N = 10^3$ in (a1) and (a2) and $N = 10^4$ in (b1) and (b2). (c) Plot of the thermodynamic order parameter $\langle \mathcal{O} \rangle_r$ versus p. Synchronized states: raster plots of spikes in (d1)–(d5), IPSR kernel estimates $R(t)$ in (e1)–(e5), and ISI histograms in (f1)–(f5) for various values of p. Plots of (g1) the average occupation degree $\langle \langle O_i \rangle \rangle_r$, (g2) the average pacing degree $\langle \langle P_i \rangle \rangle_r$, and (g3) the statistical–mechanical spiking measure $\langle M_s \rangle_r$ versus p.

population frequency $f_p \simeq 123$ Hz, corresponding to an ultrafast rhythm (100–200 Hz). In contrast to this ultrafast rhythm, individual interneurons show intermittent and stochastic discharges like Geiger counters. We collect 10^5 ISIs from all interneurons, and obtain the ISI histograms which are shown in Fig. 4(f1)–(f5). Individual interneurons show stochastic phase lockings [i.e., intermittent spikings phase-locked to $R(t)$ at random multiples of the global period T_G of $R(t)$], leading to stochastic spike skipping. Hence, multiple peaks appear at multiples of T_G ($\simeq 8.1$ ms) in the ISI histograms. With increasing p, merged multiple peaks begin to be separated, and for $p > \tilde{p}$ nearly the same histograms with clearly separated multiple peaks emerge. Hence, with increasing p the pacing degree between spikes becomes higher, and for $p > \tilde{p}$ it becomes nearly the same. For all these values of p, the population-averaged MFR $\langle f_i \rangle$, corresponding to the inverse of the average ISI, is 34 Hz. Hence, each interneuron exhibits an average firing sparsely once during about 3.6 population cycles. As a result, for $p > p^*$ fast sparsely synchronized rhythms appear.

For $p > p^*$, we characterize FSS by varying p in terms of the average occupation degree $\langle \langle O_i \rangle \rangle_r$, the average pacing degree $\langle \langle P_i \rangle \rangle_r$, and the statistical–mechanical spiking measure $\langle M_s \rangle_r$. Fig. 4(g1)–(g3) show plots of $\langle \langle O_i \rangle \rangle_r$, $\langle \langle P_i \rangle \rangle_r$, and $\langle M_s \rangle_r$, respectively. The average occupation degree $\langle \langle O_i \rangle \rangle_r$ is nearly the same ($\langle \langle O_i \rangle \rangle_r \simeq 0.28$), independently of p; only a fraction (about 1/3.6) of total interneurons fire in each stripe. This sparse occupation results

from stochastic spike skipping of individual interneurons which is well seen in the multi-peaked ISI histograms. Hence, $\langle\langle O_i\rangle\rangle_r$ characterizes the sparseness degree of FSS well. In contrast, with increase in p, at first the average pacing degree $\langle\langle P_i\rangle\rangle_r$ makes a rapid increase due to appearance of long-range connections. However, the value of $\langle\langle P_i\rangle\rangle_r$ becomes saturated at $p = \tilde{p}$ because the number of long-range connections which appear up to $\tilde{p}$ is enough to obtain maximal pacing degree. As in the case of $\langle\langle P_i\rangle\rangle_r$, the statistical–mechanical spiking measure $\langle M_s\rangle_r$ increases rapidly up to $p = \tilde{p}$ because $\langle\langle O_i\rangle\rangle_r$ is nearly independent of p. $\langle M_s\rangle_r$ is nearly equal to $\langle\langle P_i\rangle\rangle_r/3.6$ because of nearly constant sparse occupation $[\langle\langle O_i\rangle\rangle_r \simeq 1/3.6]$.

3.2. Effect of iSTDP on FSS

In this subsection, we study the effect of iSTDP on FSS [occurring for $D_{th}(\simeq 65) < D < D^*(\simeq 558)$ in the absence of iSTDP]. The initial values of synaptic strengths $\{J_{ij}\}$ are chosen from the Gaussian distribution with the mean J_0 (= 700) and the standard deviation σ_0 (=5). Then, J_{ij} for each synapse is updated according to a nearest-spike pair-based STDP rule of Eq. (7).
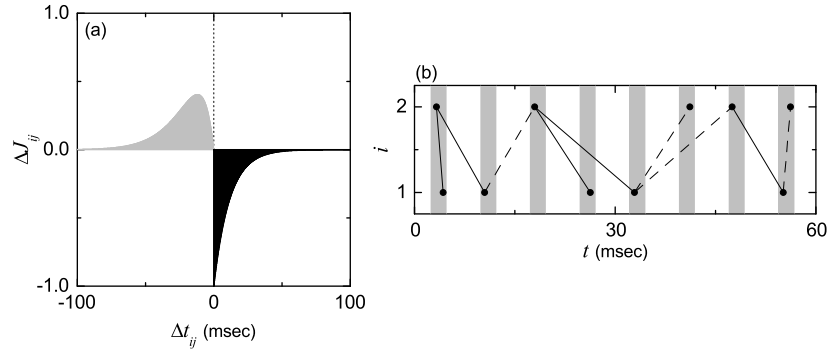
Fig. 5(a) shows an asymmetric anti-Hebbian time window for the synaptic modification $\Delta J_{ij}(\Delta t_{ij})$ of Eq. (8) versus Δt_{ij}. $\Delta J_{ij}(\Delta t_{ij})$ varies depending on the relative time difference $\Delta t_{ij} (= t_i^{(post)} - t_j^{(pre)})$ between the nearest spike times of the post-synaptic neuron i and the pre-synaptic neuron j. In contrast to the case of a Hebbian time window for the eSTDP (Kim & Lim, 2018c), when a post-synaptic spike follows a pre-synaptic spike (i.e., Δt_{ij} is positive), LTD of synaptic strength appears; otherwise (i.e., Δt_{ij} is negative), LTP occurs. A schematic diagram for the nearest-spike pair-based STDP rule is given in Fig. 5(b), where $i = 1$ and 2 correspond to the post- and the pre-synaptic interneurons. Here, gray boxes denote stripes in the raster plot, and spikes in the stripes are denoted by solid circles. When the post-synaptic neuron ($i = 1$) fires a spike, LTD (represented by solid lines) occurs through iSTDP between the post-synaptic spike and the previous nearest pre-synaptic spike. On the other hand, when the pre-synaptic neuron ($i = 2$) fires a spike, LTP (denoted by dashed lines) occurs via iSTDP between the pre-synaptic spike and the previous nearest post-synaptic spike. For the case of sparse synchronization, individual interneurons make stochastic spike skipping (i.e., they make intermittent and stochastic discharges). As a result of stochastic spike skipping, nearest-neighboring pre- and post-synaptic spikes may appear in any two separate stripes (e.g., nearest-neighboring, next-nearest-neighboring or farther-separated stripes), as well as in the same stripe, in contrast to the case of full synchronization where they appear in the same or just in the nearest-neighboring stripes [compare Fig. 5(b) with Fig. 4(b) (corresponding to the case of full synchronization) in Kim and Lim (2018c)]. For simplicity, only the cases, corresponding to the same, the nearest-neighboring, and the next-nearest-neighboring stripes, are shown in Fig. 5(b).

Fig. 6(a) shows time-evolutions of population-averaged synaptic strengths $\langle J_{ij}\rangle$ for various values of D in the SWN with $p = 0.25$; $\langle\cdots\rangle$ represents an average over all synapses. For each case of $D = 150$, 250, and 350, $\langle J_{ij}\rangle$ decreases monotonically below its initial value J_0 (=700), and it approaches a saturated limit value $\langle J_{ij}^*\rangle$ nearly at $t = 1000$ s. Consequently, LTD occurs for these values of D. On the other hand, for $D = 450$ $\langle J_{ij}\rangle$ increases monotonically above J_0, and approaches a saturated limit value $\langle J_{ij}^*\rangle$. As a result, LTP occurs for the case of $D = 450$. Histograms for fraction of synapses versus J_{ij}^* (saturated limit values of J_{ij} at $t = 1000$ s) are shown in black color for various values of D in Fig. 6(b1)–(b4); the bin size for each histogram is 10. For comparison, initial distributions of synaptic strengths $\{J_{ij}\}$ (i.e., Gaussian distributions whose mean J_0 and standard deviation σ_0 are 700 and 5, respectively) are also shown in gray color. For the cases of LTD ($D = 150$, 250, and 350), their
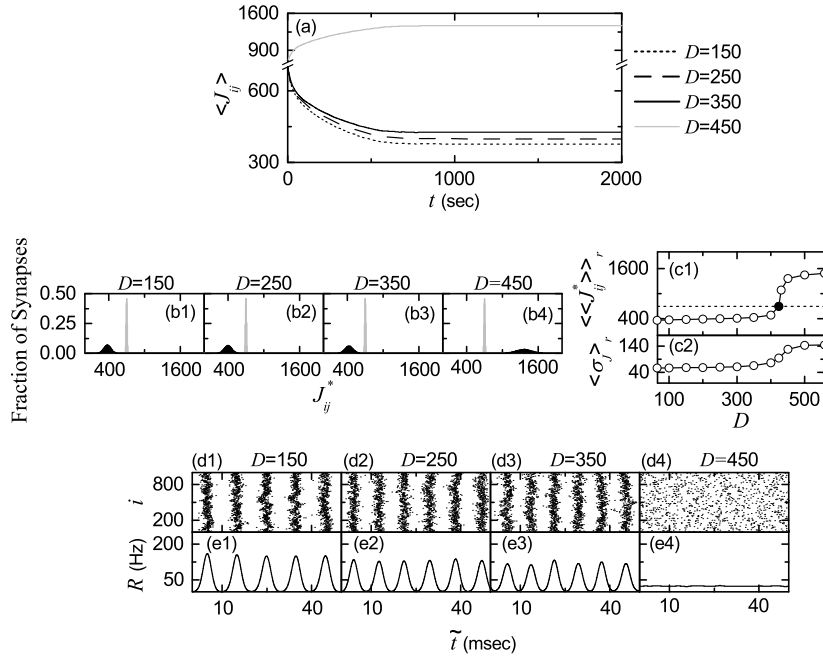
black histograms lie on the left side of the initial gray histograms, and hence their population-averaged values $\langle J_{ij}^*\rangle$ become smaller than the initial value J_0. On the other hand, the black histogram for the case of LTP ($D = 450$) is shifted to the right side of the initial gray histogram, and hence its population-averaged value $\langle J_{ij}^*\rangle$ becomes larger than J_0. For both cases of LTD and LTP, their black histograms are much wider than the initial gray histograms [i.e., the standard deviations σ_J are very larger than the initial one σ_0]. Fig. 6(c1) shows a plot of population-averaged limit values of synaptic strengths $\langle\langle J_{ij}^*\rangle\rangle_r$ versus D. Here, the horizontal dotted line represents the initial average value of coupling strengths J_0, and the threshold value $\tilde{D}$ ($\simeq 423$) for LTD/LTP (where $\langle\langle J_{ij}^*\rangle\rangle_r = J_0$) is represented by a solid circle. Hence, LTD occurs in a larger range of FSS ($D_{th}(\simeq 65) < D < \tilde{D}$); FSS in the absence of iSTDP appears in the range of $D_{th} < D < D^*(\simeq 558)$. As D is decreased from $\tilde{D}$, $\langle\langle J_{ij}^*\rangle\rangle_r$ decreases monotonically. In contrast, LTP takes place in a smaller range of FSS (i.e., $\tilde{D} < D < D^*$), and with increasing D from $\tilde{D}$ $\langle\langle J_{ij}^*\rangle\rangle_r$ increases monotonically. Fig. 6(c2) also shows plots of standard deviations $\langle\sigma_J\rangle_r$ versus D. All the values of $\langle\sigma_J\rangle_r$ are much larger than the initial values σ_0 (=5). The effects of LTD and LTP on FSS after the saturation time ($t = 1000$ s) may be well shown in the raster plot of spikes and the corresponding IPSR kernel estimate $R(t)$. Fig. 6(d1)–(d4) and (e1)–(e4) show raster plots of spikes and the IPSR kernel estimates $R(t)$ for various values of D, respectively. When compared with Fig. 2(b2)–(b5) and (c2)–(c5) in the absence of STDP, the degrees of FSS for the case of LTD ($D = 150$, 250, and 350) are increased (i.e., the amplitudes of $R(t)$ are increased) due to decreased mean synaptic inhibition. On the other hand, in the case of LTP ($D = 450$) the population state becomes desynchronized (i.e., $R(t)$ becomes nearly stationary) because of increased mean synaptic inhibition. Due to inhibition, the roles of LTD and LTP in inhibitory synaptic plasticity are reversed in comparison with those in excitatory synaptic plasticity where the degree of population synchronization is increased (decreased) via LTP (LTD) (Kim & Lim, 2018c).

In the presence of iSTDP, we also characterize individual and population behaviors for FSS (where individual firing activities differ markedly from population oscillatory behaviors) after the saturation time ($t = 1000$ s) in the range of $D_{th}(\simeq 65) < D < D^{**}(\simeq 426)$ (where FSS persists in the presence of iSTDP). For comparison, corresponding quantities for FSS in the absence of iSTDP are also given in the range of $D_{th} < D < D^*(\simeq 558)$ (where FSS appears in the absence of iSTDP). Fig. 7(a1) shows plots of the population frequency $\langle f_p\rangle_r$ of the IPSR $R(t)$ (open circles) and the population-averaged MFR $\langle\langle f_i\rangle\rangle_r$ of individual interneurons (open triangles) versus D; $\langle f_p\rangle_r$ (solid circles) and $\langle\langle f_i\rangle\rangle_r$ (solid triangles) in the absence of iSTDP are also shown. With decreasing D from D^* to D_{th}, $\langle f_p\rangle_r$ and $\langle\langle f_i\rangle\rangle_r$ in the absence of iSTDP approach each other (through decrease in $\langle f_p\rangle_r$ and increase in $\langle\langle f_i\rangle\rangle_r$), and eventually they merge for $D = D_{th}$. As a result, for $D \leq D_{th}$ full synchronization with $\langle f_p\rangle_r = \langle\langle f_i\rangle\rangle_r$ appears in the absence of iSTDP. In the presence of iSTDP, the values of $\langle f_p\rangle_r$ (open circles) are larger than those (solid circles) in the absence of iSTDP mainly due to decreased mean synaptic inhibition $\langle J_{ij}\rangle$ (i.e., LTD). As D is decreased from D^{**}, $\langle f_p\rangle_r$ (open circles) decreases. However, from $D \sim 100$ it begins to increase slowly, and then its difference from the value (solid circles) in the absence of iSTDP increases. For $D > 150$, values of $\langle\langle f_i\rangle\rangle_r$ (open triangles) are much larger than those (solid triangles) in the absence of iSTDP mainly because of LTD (i.e., decreased mean synaptic inhibition $\langle J_{ij}\rangle$). With decreasing from $D = 150$, $\langle\langle f_i\rangle\rangle_r$ (open triangle) begins to decrease slowly, in contrast to increase in $\langle\langle f_i\rangle\rangle_r$ (solid triangle) for the case without iSTDP. For $D \sim 75$ they cross, and then the values of $\langle\langle f_i\rangle\rangle_r$ (open triangles) become a little smaller than those (solid triangles) in the absence of iSTDP. Consequently, for $D = D_{th}$ the difference between $\langle f_p\rangle_r$ (open circle) and $\langle\langle f_i\rangle\rangle_r$ (open triangle) is non-zero

Fig. 5. (a) Time window for the Anti-Hebbian iSTDP. Plot of synaptic modification ΔJ_{ij} versus $\Delta t_{ij} (= t_i^{(post)} - t_j^{(pre)})$ for $A_+ = 1$, $A_- = 1.1$, $\tau_+ = 11.5$ ms and $\tau_- = 12$ ms. $t_i^{(post)}$ and $t_j^{(pre)}$ are spiking times of the ith post-synaptic and the jth pre-synaptic neurons, respectively. (b) Schematic diagram for the nearest-spike pair-based STDP rule; $i = 1$ and 2 correspond to the post- and the pre-synaptic neurons. Gray boxes and solid circles denote stripes and spikes, respectively. Solid and dashed lines denote LTD and LTP, respectively.
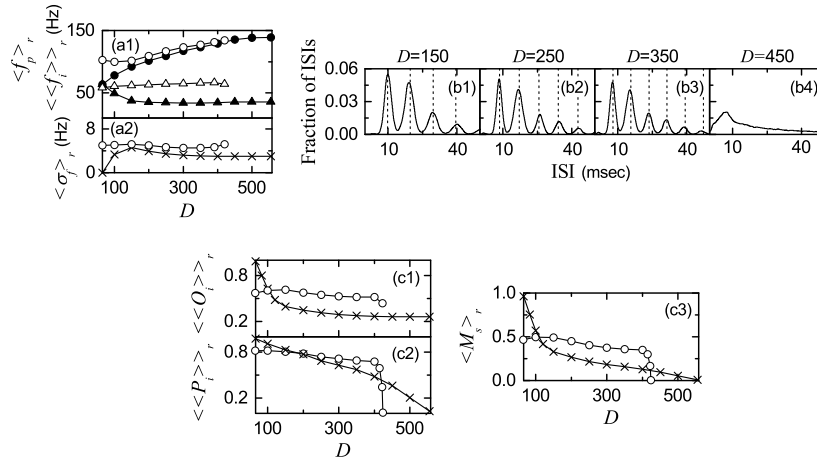

Fig. 6. Effects of iSTDP on FSS. (a) Time-evolutions of population-averaged synaptic strengths $\langle J_{ij}\rangle$ for various values of D. (b1)–(b4) Histograms for the fraction of synapses versus J_{ij}^* (saturated limit values of J_{ij} at $t = 1000$ s) are shown in black color for various values of D; for comparison, initial distributions of synaptic strengths $\{J_{ij}\}$ are also shown in gray color. Plots of (c1) population-averaged limit values of synaptic strengths $\langle\langle J_{ij}^*\rangle\rangle_r$ (open circles) and (c2) standard deviations $\langle\sigma_J\rangle_r$ (open circles) versus D. Raster plots of spikes in (d1)–(d4) and IPSR kernel estimates $R(t)$ in (e1)–(e4) for various values of D after the saturation time, where $t = t^*$ (saturation time = 1000 s) + $\tilde{t}$.

(i.e., $\langle f_p\rangle_r > \langle\langle f_i\rangle\rangle_r$), in contrast to the case without iSTDP (where the difference becomes zero). This tendency persists for $D < D_{th}$, and hence full synchronization (with $\langle f_p\rangle_r = \langle\langle f_i\rangle\rangle_r$ for $0 \le D \le D_{th}$) in the case without iSTDP breaks up into FSS (with $\langle f_p\rangle_r > \langle\langle f_i\rangle\rangle_r$) in the presence of iSTDP. Fig. 7(a2) also shows a plot of the standard deviation $\langle\sigma_f\rangle_r$ (open circles) for the distribution of MFRs of individual interneurons versus D; crosses represent $\langle\sigma_f\rangle_r$ in the absence of iSTDP. Values of $\langle\sigma_f\rangle_r$ (open circles) are larger than those (crosses) in the absence of iSTDP mainly due to increased standard deviation $\langle\sigma_J\rangle_r$ of synaptic strengths. Particularly, near D_{th} their differences become much larger because $\langle\sigma_f\rangle_r$ in the absence of iSTDP tends to converge to zero (i.e., $\langle\sigma_f\rangle_r = 0$ in the case of full synchronization for $D = D_{th}$ without iSTDP). This big difference in $\langle\sigma_f\rangle_r$ near D_{th} in the presence of iSTDP results from the break-up of full synchronization for $D \le D_{th}$ due to the dominant effect of large dispersions in synaptic inhibition.

For the case of FSS, stochastic phase locking, leading to stochastic spike skipping, is well shown in the ISI histogram with multiple peaks appearing at multiples of the global period T_G of the IPSR $R(t)$,

as shown in Fig. 7(b1)–(b3). Due to the stochastic spike skipping, sparse occupation occurs in stripes in the raster plot of spikes. As a result, the ensemble-averaged MFR $\langle f_i\rangle$ of individual interneurons becomes less than the population frequency f_p. In comparison with those for the case without iSTDP [see Fig. 2(f2)–(f4)], the peaks are shifted a little to the left, and the heights of the 1st and the 2nd peaks are increased. Hence, the average ISI $\langle ISI\rangle$ becomes shorter in the presence of iSTDP, which results in increase in the population-averaged MFRs $\langle f_i\rangle$. For the cases of $D = 350$ and 250, peaks in the presence of iSTDP are clearer than those in the absence of iSTDP, mainly due to decreased synaptic inhibition $\langle J_{ij}\rangle$ (i.e., LTD), and hence the pacing between spikes in the raster plots are increased for the case with iSTDP. On the other hand, for a smaller case of $D = 150$ a little merging between peaks occurs in the presence of iSTDP, mainly because of the dominant effect of increased standard deviation σ_J (overcoming the effect of LTD), and hence the pacing between spikes is decreased a little. For the case of desynchronized states for $D > D^{**}$, complete overlap between multiple peaks

Fig. 7. Characterization of individual and population behaviors for FSS after the saturation time ($t = 1000$ s) in the presence of iSTDP. (a1) Plots of population frequency $\langle f_p \rangle_r$ (open circles) and population-averaged MFR $\langle\langle f_i \rangle\rangle_r$ (open triangles); for comparison, $\langle f_p \rangle_r$ (solid circles) and $\langle\langle f_i \rangle\rangle_r$ (solid triangles) in the absence of iSTDP are also shown. (a2) Plot of standard deviation $\langle \sigma_f \rangle_r$ (open circles) for the distribution of MFRs of individual interneurons versus D; crosses represent $\langle \sigma_f \rangle_r$ in the absence of iSTDP. (b1)–(b4) ISI histograms for various values of D; vertical dotted lines represent multiples of the global period T_G of the IPSR $R(t)$. Plots of (c1) the average occupation degree $\langle\langle O_i \rangle\rangle_r$ (open circles), (c2) the average pacing degree $\langle\langle P_i \rangle\rangle_r$ (open circles), and (c3) the statistical–mechanical spiking measure $\langle M_s \rangle_r$ (open circles) versus D. For comparison, $\langle\langle O_i \rangle\rangle_r$, $\langle\langle P_i \rangle\rangle_r$, and $\langle M_s \rangle_r$ in the absence of iSTDP are also denoted by crosses.
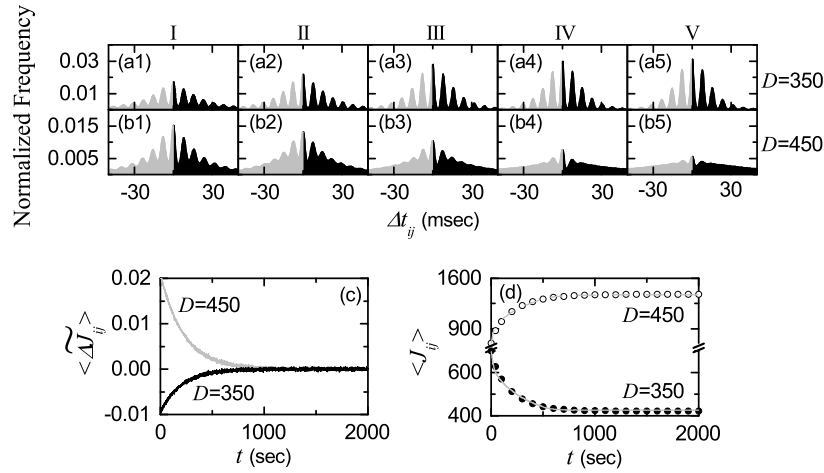
occurs [e.g., see the case of $D = 450$ in Fig. 7(b4)], and hence spikes in the raster plot are completely scattered, as shown in Fig. 6(d4).

Fig. 7(c1)–(c2) show the average occupation degree $\langle\langle O_i \rangle\rangle_r$ and the average pacing degree $\langle\langle P_i \rangle\rangle_r$ (represented by open circles), respectively; for comparison, $\langle\langle O_i \rangle\rangle_r$ and $\langle\langle P_i \rangle\rangle_r$ (denoted by crosses) are also shown in the case without iSTDP. In most cases of LTD, the values of $\langle\langle O_i \rangle\rangle_r$ (open circles) are larger than those (crosses) in the absence of iSTDP, due to decreased mean synaptic inhibition. With decreasing D from D^{**}, there are no particular variations in $\langle\langle O_i \rangle\rangle_r$ (open circles). On the other hand, $\langle\langle O_i \rangle\rangle_r$ (crosses) in the absence of iSTDP increases rapidly to 1 near D_{th}, because of existence of full synchronization for $D \leq D_{th}$ with $\langle\langle O_i \rangle\rangle_r = 1$. Hence, near D_{th}, the values (open circles) of $\langle\langle O_i \rangle\rangle_r$ in the presence of iSTDP are smaller than those (crosses) for the case without iSTDP due to the dominant effect of standard deviations of synaptic inhibition strengths (causing break up of full synchronization in the absence of iSTDP). Next, we consider the average pacing degree $\langle\langle P_i \rangle\rangle_r$. As D is increased from D_{th} to D^*, $\langle\langle P_i \rangle\rangle_r$ (crosses) in the absence of iSTDP decreases smoothly. On the other hand, $\langle\langle P_i \rangle\rangle_r$ in the presence of iSTDP shows a step-like transition. In the region of LTD, there are no particular variations in $\langle\langle P_i \rangle\rangle_r$ (just a little decrease with increasing D). Near $\tilde{D}(\simeq 423)$, a rapid transition to the case of $\langle\langle P_i \rangle\rangle_r = 0$ occurs due to LTP (i.e., increased mean synaptic inhibition), in contrast to the smooth decrease in $\langle\langle P_i \rangle\rangle_r$ (crosses) in the absence of iSTDP. For $\sim 200 < D < \tilde{D}$, the values of $\langle\langle P_i \rangle\rangle_r$ (open circles) are larger than those (crosses) in the case without iSTDP mainly because of LTD (i.e., decreased mean synaptic inhibition). However, for $D_{th} < D <\sim 200$ the values (open circles) of $\langle\langle P_i \rangle\rangle_r$ in the presence of iSTDP are smaller than those (crosses) for the case without iSTDP mainly because of the dominant effect of standard deviations of synaptic inhibition strengths.

The statistical–mechanical spiking measure $\langle M_s \rangle_r$ (combining the effect of both the average occupation and pacing degrees) is represented by open circles in Fig. 7(c3). With decreasing from D^* $\langle M_s \rangle_r$ in the absence of iSTDP (denoted by crosses) increases smoothly, and near $D \sim 100$ it begins to increase rapidly due to existence of full synchronization for $D = D_{th}$. In contrast, in the presence of iSTDP, $\langle M_s \rangle_r$ shows a step-like transition (see open circles). Due to the effect of $\langle\langle P_i \rangle\rangle_r$, a rapid transition to the case of $\langle M_s \rangle_r = 0$ occurs near $\tilde{D}$ because of LTP (decreasing the degree of FSS). On the other hand, in most cases of LTD ($\sim 100 < D < \tilde{D}$), the values of $\langle M_s \rangle_r$ (open circles) are larger than those (crosses) in the case without iSTDP mainly because of LTD (increasing the degree

of FSS). However, for $D_{th} < D <\sim 100$ the values (open circles) of $\langle M_s \rangle_r$ in the presence of iSTDP are smaller than those (crosses) for the case without iSTDP mainly due to the dominant effect of standard deviations of synaptic inhibition strengths (decreasing the degree of FSS). As a result, in most cases of LTD (increasing the degree of FSS), good synchronization with higher $\langle M_s \rangle_r$ gets better; in some other cases near D_{th} the degree of good synchronization decreases mainly due to the dominant effect of standard deviation (decreasing the degree of FSS) of synaptic inhibition strengths. On the other hand, in all cases bad synchronization with lower $\langle M_s \rangle_r$ gets worse via LTP (decreasing the degree of FSS). This kind of Matthew effect (valid in most cases of LTD) in inhibitory synaptic plasticity is in contrast to the Matthew effect in excitatory synaptic plasticity where good (bad) synchronization gets better (worse) via LTP (LTD) (Kim & Lim, 2018b, c); the roles of LTD and LTP in the presence of iSTDP are reversed in comparison to those in the case of eSTDP.

From now on, we make an intensive investigation on emergences of LTD and LTP of synaptic strengths via a microscopic method based on the distributions of time delays $\{\Delta t_{ij}\}$ between the pre- and the post-synaptic spike times. Fig. 8(a1)–(a5) and (b1)–(b5) show time-evolutions of normalized histograms $H(\Delta t_{ij})$ for the distributions of time delays $\{\Delta t_{ij}\}$ for $D = 350$ and 450, respectively; the bin size in each histogram is 0.5 ms. Here, we consider 5 stages, represented by I (starting from 0 s), II (starting from 100 s), III (starting from 300 s), IV (starting from 500 s), and V (starting from 800 s). At each stage, we get the distribution of $\{\Delta t_{ij}\}$ for all synaptic pairs during 0.2 s and obtain the normalized histogram by dividing the distribution with the total number of synapses (=50000). For $D = 350$ (LTD), multi-peaks appear in each histogram, in contrast to the case of full synchronization (Kim & Lim, 2018c). As explained in Fig. 5(b), due to stochastic spike skipping, nearest-neighboring pre- and post-synaptic spikes appear in any two separate stripes (e.g., nearest-neighboring, next-nearest-neighboring or farther-separated stripes), as well as in the same stripe, which is similar to the multi-peaked ISI histogram. In the stage I, in addition to the main central (1st-order) peak, higher kth-order ($k = 2, \ldots, 7$) left and right minor peaks also are well seen. Here, LTD and LTP occur in the black ($\Delta t > 0$) and the gray ($\Delta t < 0$) parts, respectively. As the time t is increased (i.e., with increase in the level of stage), peaks become narrowed, and then they become sharper. Particularly, heights of major ($k = 1, 2, 3, 4$) peaks tend to be increased, while those of minor ($k = 5, 6, 7$)

Fig. 8. Microscopic investigations on emergences of LTD and LTP. Time-evolutions of the normalized histogram $H(\Delta t_{ij})$ for the distributions of time delays $\{\Delta t_{ij}\}$ between the pre- and the post-synaptic spike times for $D = 350$ in (a1)–(a5) and for $D = 450$ in (b1)–(b5); 5 stages are shown in I (starting from 0 s), II (starting from 100 s), III (starting from 300 s), IV (starting from 500 s), and V (starting from 800 s). (c) Time-evolutions of multiplicative synaptic modification $\langle \widetilde{\Delta J_{ij}} \rangle$ for $D = 350$ (black line) and $D = 450$ (gray line). (d) Time-evolutions of population-averaged synaptic strength $\langle J_{ij} \rangle$ (obtained by an approximate method) for $D = 350$ (solid circle) and $D = 450$ (open circle); gray solid and dashed lines represent ones (obtained by direct calculations) for $D = 350$ and 450 in Fig. 6(a), respectively.

peaks seem to be decreased. Intervals between peaks also seem to be decreased a little because the population frequency f_p of $R(t)$ increases a little with the stage. In the stage I, the effect in the right black part (LTD) is dominant, in comparison with the effect in the left gray part (LTP), and hence the overall net LTD begins to emerge. As the level of stage is increased, the effect of LTD in the black part tends to nearly cancel out the effect of LTP in the gray part at the stage V. For $D = 450$ (LTP), in the initial stage I, multi-peaks are well seen in the histogram, like the case of $D = 350$. For this initial stage, the effect in the left gray part (LTP) is dominant, in comparison with the effect in the right black part (LTD), and hence the overall net LTP begins to emerge. However, with increasing the level of stage, peaks become wider and the tendency of merging between the peaks is more and more intensified, in contrast to the case of $D = 350$. Furthermore, the effect of LTP in the gray part tends to nearly cancel out the effect of LTD in the black part at the stage V.

We consider successive time intervals $I_k \equiv (t_k, t_{k+1})$, where $t_k = 0.2 \cdot (k - 1)$ s ($k = 1, 2, 3, \dots$). With increasing the time t, in each kth time interval I_k, we obtain the kth normalized histogram $H_k(\Delta t_{ij})$ ($k = 1, 2, 3, \dots$) through the distribution of $\{\Delta t_{ij}\}$ for all synaptic pairs during 0.2 s. Then, from Eq. (7), we get the population-averaged synaptic strength $\langle J_{ij} \rangle_k$ recursively:

$$\langle J_{ij} \rangle_k = \langle J_{ij} \rangle_{k-1} + \delta \cdot \langle \widetilde{\Delta J_{ij}(\Delta t_{ij})} \rangle_k, \tag{16}$$

where $\langle J_{ij} \rangle_0 = J_0$ (=700: initial mean value), $\langle \cdots \rangle_k$ means the average over the distribution of time delays $\{\Delta t_{ij}\}$ for all synaptic pairs in the kth time interval, and the multiplicative synaptic modification $\widetilde{\Delta J_{ij}(\Delta t_{ij})}$ is given by the product of the multiplicative factor $(J^* - J_{ij})$ [J_{ij}: synaptic coupling strength at the $(k-1)$th stage] and the absolute value of synaptic modification $|\Delta J_{ij}(\Delta t_{ij})|$:

$$\widetilde{\Delta J_{ij}(\Delta t_{ij})} = (J^* - J_{ij}) |\Delta J_{ij}(\Delta t_{ij})|. \tag{17}$$

Here, we obtain the population-averaged multiplicative synaptic modification $\langle \widetilde{\Delta J_{ij}(\Delta t_{ij})} \rangle_k$ for the kth stage via a population-average approximation where J_{ij} is replaced by its population average $\langle J_{ij} \rangle_{k-1}$ at the $(k-1)$th stage:

$$\langle \widetilde{\Delta J_{ij}(\Delta t_{ij})} \rangle_k \simeq (J^* - \langle J_{ij} \rangle_{k-1}) \langle |\Delta J_{ij}(\Delta t_{ij})| \rangle_k. \tag{18}$$
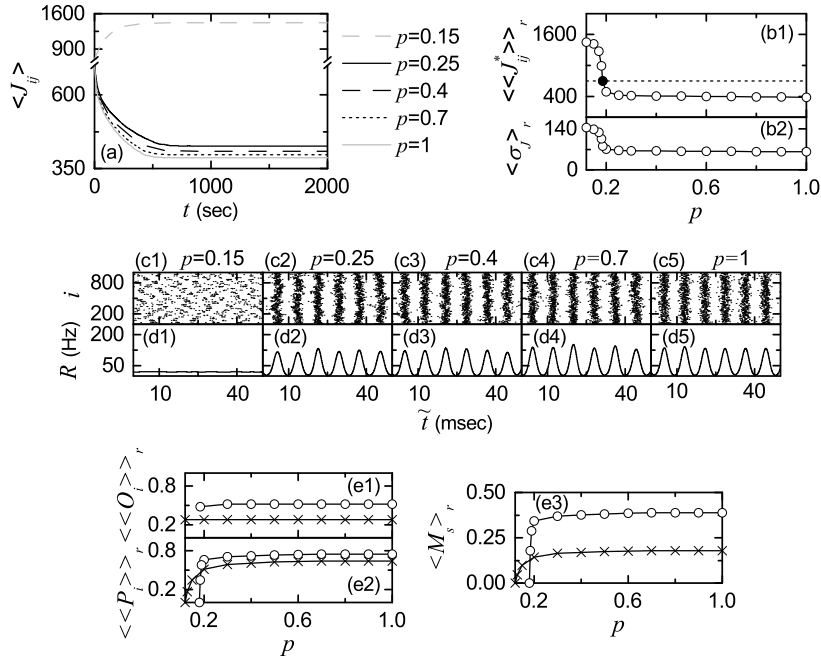
Here, $\langle |\Delta J_{ij}(\Delta t_{ij})| \rangle_k$ may be easily obtained from the kth normalized histogram $H_k(\Delta t_{ij})$:

$$\langle |\Delta J_{ij}(\Delta t_{ij})| \rangle_k \simeq \sum_{\text{bins}} H_k(\Delta t_{ij}) \cdot |\Delta J_{ij}(\Delta t_{ij})|. \tag{19}$$

Using Eqs. (16), (18), and (19), we obtain approximate values of $\langle \widetilde{\Delta J_{ij}} \rangle_k$ and $\langle J_{ij} \rangle_k$ in a recursive way. Fig. 8(c) shows time-evolutions of $\langle \widetilde{\Delta J_{ij}} \rangle$ for $D = 350$ (black curve) and $D = 450$ (gray curve). $\langle \widetilde{\Delta J_{ij}} \rangle$ for $D = 350$ is negative, while $\langle \widetilde{\Delta J_{ij}} \rangle$ for $D = 450$ is positive. For both cases they converge toward nearly zero at the stage V (starting from 800 s) because the effects of LTD and LTP in the normalized histograms are nearly canceled out. The time-evolutions of $\langle J_{ij} \rangle$ for $D = 350$ (solid circles) and $D = 450$ (open circles) are also shown in Fig. 8(d). We note that the approximately-obtained values for $\langle J_{ij} \rangle$ agree well with directly-obtained ones [denoted by the gray solid (dashed) line for $D = 350$ (450)] in Fig. 6(a). Consequently, LTD (LTP) emerges for $D = 350$ (450).

Finally, we investigate the effect of network architecture on FSS for $D = 350$ by varying the rewiring probability p in the presence of iSTDP; in the absence of iSTDP, FSS appears for $p > p^*(\simeq 0.12)$. Fig. 9(a) shows time-evolutions of population-averaged synaptic strengths $\langle J_{ij} \rangle$ for various values of p. For each case of $p = 0.25$, 0.4, 0.7, and 1.0, $\langle J_{ij} \rangle$ decreases monotonically below its initial value J_0 (=700), and it approaches a saturated limit value $\langle J_{ij}^* \rangle$ nearly at $t = 1000$ s. As a result, LTD occurs for these values of p. On the other hand, for $p = 0.15$ $\langle J_{ij} \rangle$ increases monotonically above J_0, and approaches a saturated limit value $\langle J_{ij}^* \rangle$. As a result, LTP occurs for the case of $p = 0.15$. Fig. 9(b1) shows a plot of population-averaged limit values of synaptic strengths $\langle \langle J_{ij}^* \rangle \rangle_r$ (J_{ij}^*: saturated limit values of J_{ij} at $t = 1000$ s) versus p. Here, the horizontal dotted line represents the initial average value of coupling strengths J_0 (= 700), and the threshold value p_{th} ($\simeq 0.185$) for LTD/LTP (where $\langle \langle J_{ij}^* \rangle \rangle_r = J_0$) is represented by a solid circle. Hence, LTD occurs in a larger range of $p > p_{th}$, while LTP takes place in a smaller range of $p^* < p < p_{th}$. Fig. 9(b2) also shows a plot of standard deviations $\langle \sigma_J \rangle_r$ versus p. All the values of $\langle \sigma_J \rangle_r$ are much larger than the initial value σ_0 (=5). The effects of LTD and LTP on FSS after the saturation time ($t = 1000$ s) may be well shown in the raster plot of spikes and the corresponding IPSR kernel estimate $R(t)$ which are shown in Fig. 9(c1)–(c5) and (d1)–(d5), respectively. In comparison with Fig. 4(d1)–(d5) and (e1)–(e5) in the absence of STDP, the degrees of FSS for the case of LTD ($p = 0.25$, 0.4, 0.7, and

Fig. 9. Effect of network architecture on FSS for $D = 350$ in the presence of iSTDP. (a) Time-evolutions of population-averaged synaptic strengths $\langle J_{ij} \rangle$ for various values of p. Plots of (b1) population-averaged limit values of synaptic strengths $\langle\langle J_{ij}^* \rangle\rangle_r$ and (b2) standard deviations $\langle \sigma_J \rangle_r$ versus p. Raster plots of spikes in (c1)–(c5) and IPSR kernel estimates $R(t)$ in (d1)–(d5) for various values of p. Plots of (e1) the average occupation degree $\langle\langle O_i \rangle\rangle_r$ (represented by open circles), (e2) the average pacing degree $\langle\langle P_i \rangle\rangle_r$ (denoted by open circles), and (e3) the statistical–mechanical spiking measure $\langle M_s \rangle_r$ (represented by open circles) versus p. For comparison, $\langle\langle O_i \rangle\rangle_r$, $\langle\langle P_i \rangle\rangle_r$, and $\langle M_s \rangle_r$ in the absence of iSTDP are also denoted by crosses.
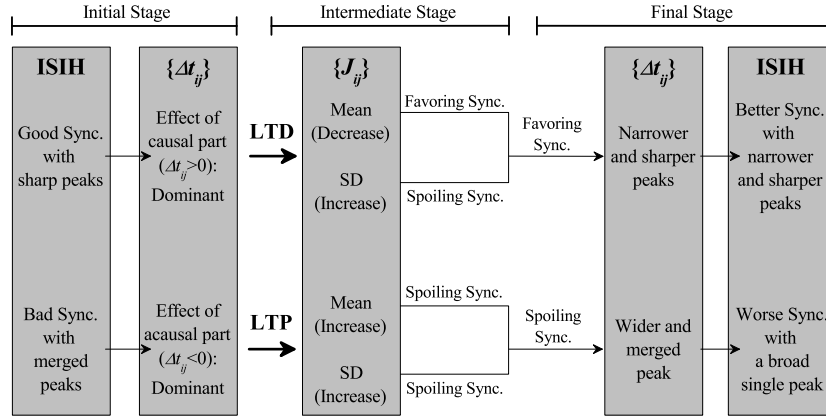
1.0) are increased (i.e., the amplitudes of $R(t)$ are increased) due to decreased mean synaptic inhibition. On the other hand, for the case of LTP ($p = 0.15$) the population state becomes desynchronized (i.e., $R(t)$ becomes nearly stationary) because of increased mean synaptic inhibition.

Fig. 9(e1) and (e2) show the average occupation degree $\langle\langle O_i \rangle\rangle_r$ and the average pacing degree $\langle\langle P_i \rangle\rangle_r$ of FSS (represented by open circles), respectively; for comparison, $\langle\langle O_i \rangle\rangle_r$ and $\langle\langle P_i \rangle\rangle_r$ (denoted by crosses) are also shown in the case without iSTDP. In the presence of iSTDP, $\langle\langle O_i \rangle\rangle_r$ (open circles) shows just a little variation, and their values are larger than those (crosses) in the absence of iSTDP, mainly due to LTD. On the other hand, $\langle\langle P_i \rangle\rangle_r$ in the presence of iSTDP shows a step-like transition. In most region of LTD, there are no particular variations in $\langle\langle P_i \rangle\rangle_r$ (just a little decrease with decreasing p), and their values are larger than those (crosses) in the absence of iSTDP mainly because of decreased mean synaptic inhibition. However, near p_{th} ($\simeq 0.185$), a rapid transition to the case of $\langle\langle P_i \rangle\rangle_r = 0$ occurs due to LTP (i.e., increased mean synaptic inhibition), in contrast to the smooth decrease in $\langle\langle P_i \rangle\rangle_r$ (crosses) in the absence of iSTDP. Fig. 9(e3) shows the statistical–mechanical spiking measure $\langle M_s \rangle_r$ (combining the effect of both the average occupation and pacing degrees and represented by open circles) in the range of $p^{**}(\simeq 0.161) < p \leq 1$ (where FSS persists in the presence of iSTDP). In the absence of iSTDP, with decreasing from $p = 1$ to $p^*(\simeq 0.12)$, $\langle M_s \rangle_r$ (denoted by crosses) decreases smoothly. In contrast, in the presence of iSTDP, $\langle M_s \rangle_r$ shows a step-like transition (see open circles). Due to the effect of $\langle\langle P_i \rangle\rangle_r$, a rapid transition to the case of $\langle M_s \rangle_r = 0$ occurs near p_{th} because of LTP (decreasing the degree of FSS). On the other hand, in most region of p, the values of $\langle M_s \rangle_r$ (open circles) are larger than those (crosses) in the case without iSTDP, mainly because of LTD (increasing the degree of FSS). As a result, good synchronization with higher $\langle M_s \rangle_r$ gets better via LTD, while bad synchronization with lower $\langle M_s \rangle_r$ gets worse via LTP. This kind of Matthew effect in inhibitory synaptic plasticity is in contrast to the Matthew effect in excitatory synaptic plasticity where good (bad) synchronization gets better (worse) via LTP (LTD) (Kim & Lim, 2018b, c).

4. Summary and discussion

We are interested in synchronized brain rhythms in health and disease (Buzsáki, 2006; Traub & Whittington, 2010). For example, synchronous neural oscillations are used for efficient sensory processing such as binding of the integrated whole image in the visual cortex via synchronization of neural firings (Gray, 1994; Gray & Singer, 1989; Singer, 1999; Singer & Gray, 1995) In addition to such neural encoding of sensory stimuli, neural synchronization is also correlated with pathological brain rhythms related to neural disease (e.g., Parkinson's disease, epilepsy, and schizophrenia) (Grosse, Cassidy, & Brown, 2002; Tass et al., 1998; Uhlhaas & Singer, 2006, 2010).

Particularly, we are concerned about fast sparsely synchronized rhythms in an inhibitory Watts–Strogatz SWN of Izhikevich FS interneurons. A neural circuit in the major parts of the brain such as thalamus, hippocampus and cortex is composed of a few types of excitatory principal cells and diverse types of inhibitory interneurons. Functional diversity of interneurons increases the computational power of principal cells (Buzsáki, 2006; Buzsáki et al., 2004). When the synaptic decay time is enough long, mutual inhibition may synchronize neural firings. By providing a coherent oscillatory output to the principal cells, the interneuronal networks play the role of the backbones (i.e., pacemakers or synchronizers) for many brain rhythms such as the 10-Hz thalamocortical spindle rhythms (Golomb & Rinzel, 1994) and the 40-Hz gamma rhythms in the hippocampus and the cortex (Wang & Buzsáki, 1996; Whittington, Traub, Kopell, Ermentrout, & Buhl, 2000). A framework for emergence of sparsely synchronized rhythms (where stochastic and intermittent single-cell firing activity is markedly different from fast population oscillation) was developed in random networks with delayed synaptic connections (Brunel, 2000; Brunel & Hakim, 1999; Brunel & Wang, 2003; Geisler et al., 2005). Each interneuron in the interneuronal network receives stochastic external excitatory synaptic inputs. When this background noise is strong, interneurons discharge irregularly as Geiger counters,

Initial Stage   Intermediate Stage   Final Stage

ISIH — Good Sync. with sharp peaks

{Δt_{ij}} — Effect of causal part ($\Delta t_{ij} > 0$): Dominant

LTD →

{J_{ij}} — Mean (Decrease) / SD (Increase)

Favoring Sync. / Spoiling Sync.

Favoring Sync.

{Δt_{ij}} — Narrower and sharper peaks

ISIH — Better Sync. with narrower and sharper peaks

ISIH — Bad Sync. with merged peaks

{Δt_{ij}} — Effect of acausal part ($\Delta t_{ij} < 0$): Dominant

LTP →

{J_{ij}} — Mean (Increase) / SD (Increase)

Spoiling Sync. / Spoiling Sync.

Spoiling Sync.

{Δt_{ij}} — Wider and merged peak

ISIH — Worse Sync. with a broad single peak

Fig. 10. Summary on the effects of iSTDP on good and bad synchronization: time-evolutions of good and bad synchronization in the presence of iSTDP. Here, synchronization and standard deviation are abbreviated as sync. and SD, respectively.

and the population state becomes desynchronized. However, as the inhibitory recurrent feedback becomes sufficiently strong, the asynchronous state becomes destabilized, and then a synchronized state with irregular and sparse neural discharges appears. In this way, under the balance between strong external random excitation and strong recurrent inhibition, FSS was found to emerge in the interneuronal network. For this case of FSS, the population frequency f_p is ultrafast (i.e. 100–200 Hz), while individual interneurons discharge stochastically at much lower rates than f_p. This type of fast sparse rhythms was experimentally observed in hippocampal sharp-wave ripples (100–200 Hz), associated with memory consolidation, during slow-wave sleep (Buzsáki, 1986; Buzsáki, Urioste, Hetke, & Wise, 1992) and in cerebellar fast oscillations (∼ 200 Hz), related to fine motor coordination of inhibitory Purkinje cells (Adrian, 1935; Shin & De Schutter, 2006).

In previous works on FSS, synaptic inhibition strengths were static (i.e., inhibitory synaptic plasticity was not considered). On the other hand, in the present work, adaptive dynamics of synaptic inhibition strengths are governed by the iSTDP (which controls the efficacy of diverse computational functions of interneurons). The effects of iSTDP on FSS have been investigated in the SWN with $p = 0.25$ by varying the noise intensity D. An asymmetric anti-Hebbian time window has been used for the iSTDP update rule, in contrast to the Hebbian time window for the case of eSTDP. Our results on the effects of iSTDP on FSS are well summarized in the diagram in Fig. 10. For the case of FSS, the ISI histogram consists of multiple peaks, due to stochastic spike skipping. These multiple peaks are sharp for the case of good synchronization (with higher spiking measure), while they are merged in the case of bad synchronization (with lower spiking measure) (see the 1st column in Fig. 10). Emergences of LTD and LTP of synaptic inhibition strengths were investigated via a microscopic method based on the distributions of time delays {Δt_{ij}} between the nearest spiking times of the pre- and the post-synaptic interneurons. Like the case of multi-peaked ISI histogram, sharp multi-peaks appear in the normalized histogram for the distribution of {Δt_{ij}}; the heights of peaks for the case of good synchronization are higher than those in the case of bad synchronization. For the case of good synchronization, the effect of causal part with $\Delta t > 0$ is dominant, and hence LTD begins to occur (see the 2nd column in Fig. 10). On the other hand, in the case of bad synchronization the effect of acausal part with $\Delta t < 0$ is dominant, and hence LTP begins to take place.

The distribution of synaptic inhibition strengths {J_{ij}} is evolved in the presence of iSTDP (see the 3rd column in Fig. 10). For the case of good synchronization, its mean $\langle J_{ij} \rangle$ is decreased (i.e., LTD occurs), while in the case of bad synchronization $\langle J_{ij} \rangle$ is increased (i.e., LTP occurs). The standard deviations σ_J for both cases of good

and bad synchronization increase. Decrease (increase) in the mean $\langle J_{ij} \rangle$ [i.e., LTD (LTP)] favors (disfavors) FSS due to increased (decreased) population-averaged MFR $\langle f_i \rangle$ of individual interneurons. Increased standard deviation σ_J leads to increase in variation of inhibitory synaptic inputs to individual interneurons, and hence distributions of MFRs of individual interneurons become broader (i.e., standard deviation σ_f for the distribution of MFRs increases). Due to increased σ_f, it becomes difficult for interneurons to keep their pacing, which results in decrease in the degree of FSS (i.e., FSS is spoiled), as in the case of increasing the noise intensity D. In this way, dispersion of synaptic inhibition strengths seems to play a role which is similar to that of noise.

For the case of iSTDP, in addition to the effect of mean value (LTP or LTD), the effect of standard deviation σ_J on population synchronization may also become significant in some cases, in contrast to the case of eSTDP where the mean of LTP/LTD was found to be always dominant (Kim & Lim, 2018b, c). For most cases of good synchronization, the effect of LTD (increasing the degree of FSS) is dominant in comparison with the effect of standard deviation σ_J (decreasing the degree of FSS). Consequently, in most cases of good synchronization, it has been found to get better via LTD; in some other cases where the effect of standard deviation σ_J is dominant (occurring near D_{th}), the degree of good synchronization decreases even in the presence of LTD. In contrast, for all cases, bad synchronization has been found to get worse via LTP (decreasing the degree of FSS). This type of Matthew effect (valid in most cases of LTD) in inhibitory synaptic plasticity is in contrast to the Matthew effect in excitatory synaptic plasticity (Kim & Lim, 2018b, c). For the case of eSTDP, LTP (LTD) has a tendency to favor (disfavor) synchronization via positive (structural) feedback, while LTD (LTP) for the case of iSTDP has a tendency favoring (disfavoring) FSS through a negative (structural) feedback. Hence, due to inhibition via negative feedback, the roles of LTD and LTP in inhibitory plasticity are reversed in comparison with those in excitatory synaptic plasticity through positive feedback where good (bad) synchronization gets better (worse) via LTP (LTD). Consequently, in most region of LTD, the degree of FSS becomes increased, and a rapid transition from FSS to desynchronization occurs via LTP, in contrast to the relatively smooth transition in the absence of iSTDP.

The process of iSTDP may be well visualized in the normalized histogram of $H(\Delta t_{ij})$ and the ISI histogram (see the 4th and 5th columns in Fig. 10). With increasing time t, peaks in the normalized histogram $H(\Delta t_{ij})$ becomes narrowed and sharper for the case of LTD, while in the case of LTP peaks become wider and merged. After a sufficient time, the effect of LTD in the right causal part with $\Delta t > 0$ nearly cancels out the effect of LTP in the left acausal part with $\Delta t < 0$. Then, saturated limit states appear

without further change in synaptic strengths. For most cases of good synchronization, peaks in the ISI histogram become clearer (i.e., narrower and sharper), mainly due to the dominant effect of decreased synaptic inhibition (i.e., LTD), and hence the pacing between spikes in the raster plot is increased. As a result, in most cases good synchronization gets better via LTD. In contrast, for the case of bad synchronization, complete overlap between peaks in the ISI histogram occurs (i.e., a broad single peak appears) due to increased synaptic inhibition (i.e., LTP), and hence spikes are completely scattered in the raster plot. Consequently, bad synchronization gets worse via LTP.

Emergences of LTD and LTP of synaptic inhibition strengths were investigated via a microscopic method based on the distributions of time delays $\{\Delta t_{ij}\}$ between the nearest spiking times of the pre- and the post-synaptic interneurons. Time evolutions of normalized histograms $H(\Delta t_{ij})$ were followed for both cases of LTD and LTP. Using a recurrence relation, we recursively obtained population-averaged synaptic inhibition strength $\langle J_{ij} \rangle$ at successive stages through an approximate calculation of population-averaged multiplicative synaptic modification $\langle \widetilde{\Delta J_{ij}} \rangle$ of Eq. (18), based on the normalized histogram at each stage. These approximate values of $\langle J_{ij} \rangle$ have been found to agree well with directly-calculated ones. Consequently, one can understand clearly how microscopic distributions of $\{\Delta t_{ij}\}$ contribute to $\langle J_{ij} \rangle$ or more directly to $\langle \widetilde{\Delta J_{ij}} \rangle$.

By varying the rewiring probability p in the SWN, we also studied the effect of network architecture on FSS in the presence of iSTDP. As in the above case of variation in D for $p = 0.25$, a Matthew effect has also been found to occur in the case of variation in p for $D = 350$. As a result, good (bad) synchronization with higher (lower) spiking measure M_s for $p > (<)p_{th} (\simeq 0.185)$ gets better (worse) via LTD (LTP).

Finally, we discuss limitations of our work and future works. In our work, we employed the standard "duplet" STDP model, based on the nearest pre- and post-synaptic spike pairs. However, unfortunately this pair-based STDP model accounts for neither the dependence of plasticity on the repetition frequency of the pairs of pre- and post-synaptic spikes, nor the results of recent triplet and quadruplet experiments (Morrison, Diesmann, & Gerstner, 2008; Pfister & Gerstner, 2006). Hence, as a future work, it would be interesting to study the effect of iSTDP on FSS by using a triplet iSTDP rule and to compare its results with those for the case of duplet iSTDP rule. Inhibitory neurons have been found to possess diverse types of plasticity rules. For example, Hebbian STDP (Fino, Deniau, & Venance, 2008; Kullmann & Lamsa, 2007), anti-Hebbian STDP (Bell, Han, Sugawara, & Grant, 1997; Fino, Glowinski, & Venance, 2005; Kullmann & Lamsa, 2007; Kullmann et al., 2012), and anti-Hebbian STDP with only LTD (Tzounopoulos et al., 2004) were observed in the case of excitatory (E) to inhibitory (I) connection. Moreover, for the case of I to E connection, anti-symmetric Hebbian STDP (Haas et al., 2006) and symmetric (non-Hebbian) STDP (Woodin et al., 2003) were found. However, in the preset work, for simplicity we assumed that all interneurons exhibit identical anti-Hebbian STDP for the case of I to I connection. To take into consideration heterogeneity on synaptic plasticity of inhibitory cells seems to be beyond the present work, and it will be left as a future work. In the present work, we considered only the interneuronal network. As explained above, a major neural circuit consists of two excitatory and inhibitory populations. In previous works (Brunel & Wang, 2003; Geisler et al., 2005), they also considered the two-population network with four (I to I, I to E, E to I, and E to E) types of connections. The additional I to E, E to I, and E to E connections have tendency to decrease the population frequency f_p. It was found that f_p was much reduced to about 30–100 Hz (corresponding to gamma rhythms), when compared with the case of pure interneuronal network. Hence, in future, it would be interesting to study the effects of interpopulation (I to E and E to I) STDP on FSS in the two-population network of inhibitory Izhikevich FS interneurons and

excitatory Izhikevich regular-spiking neurons, in addition to the studied intrapopulation (E to E and I to I) STDP. In our work, we also considered just the spiking neurons. In addition to spiking, bursting is also another type of neuronal firing activities. Burstings occur when neuronal activity alternates, on a slow timescale, between a silent phase and an active (bursting) phase of fast repetitive spikings. There are several representative examples of bursting neurons. Recently, we also investigated the effect of iSTDP on burst synchronization in a scale-free neuronal network of inhibitory Hindmarsh–Rose bursting neurons (Kim & Lim, 2018a). Thus, the effect of iSTDP on burst synchronization was also found to be in contrast to the effect of eSTDP on burst synchronization, similar to the case of spiking neurons. Finally, we note that there exist some limitations to STDP in views of biological contexts (Markram, Gerstner, & Sjöström, 2011). For example, STDP has been questioned as a general model of synaptic plasticity (Lisman & Spruston, 2010), the classic STDP windows for LTP and LTD were found to be only one of many possible ones (olde Scheper, Meredith, Mansvelder, van Pelt, & van Ooyen, 2018), and because of the attenuation of the back-propagating action potential, STDP was found to depend on the dendritic synapse location (Froemke, Tsay, Raad, Long, & Dan, 2006; Letzkus, Kampa, & Stuart, 2006; Sjöström & Häusser, 2006). In the presence of these limitations, we expect that our results on inhibitory synaptic plasticity of I to I connections would make some contributions for understanding the effects of iSTDP on fast sparsely synchronized rhythms

References

Abbott, L. F., & Blum, K. I. (1996). Functional significance of long-term potentiation for sequence learning and prediction. *Cerebral Cortex*, 6, 406–416.

Abbott, L. F., & Nelson, S. B. (2000). Synaptic plasticity: taming the beast. *Nature Neuroscience*, 3, 1178–1183.

Achard, S., & Bullmore, E. T. (2007). Efficiency and cost of economical brain functional networks. *PLoS Computational Biology*, 3, e17.

Adrian, E. (1935). Discharge frequencies in the cerebral and cerebella cortex. *Proceedings of Physical Society*, 83, 32–33.

Bassett, D. S., & Bullmore, E. (2006). Small-world brain networks. *The Neuroscientist*, 12, 512–523.

Bell, C. C., Han, V. Z., Sugawara, Y., & Grant, K. (1997). Synaptic plasticity in a cerebellum-like structure depends on temporal order. *Nature*, 387, 278–281.

Bi, G.-Q., & Poo, M.-M. (1998). Synaptic modifications in cultured hippocampal neurons: dependence on spike timing, synaptic strength, and postsynaptic cell type. *The Journal of Neuroscience*, 18, 10464–10472.

Bi, G.-Q., & Poo, M.-M. (2001). Synaptic modification by correlated activity: Hebb's postulate revisited. *Annual Review of Neuroscience*, 24, 139–166.

Bienenstock, E. L., Cooper, L. N., & Munro, P. W. (1982). Theory for the development of neuron selectivity: orientation specificity and binocular interaction in visual cortex. *The Journal of Neuroscience*, 2, 32–48.

Blum, K. I., & Abbott, L. F. (1996). A model of spatial map formation in the hippocampus of the rat. *Neural Computation*, 8, 85–93.

Borges, R. R., Borges, F. S., Batista, A. M., Lameu, E. L., Viana, R. L., Iarosz, K. C., et al. (2016). Effects of spike timing-dependent plasticity on the synchronization in a random Hodgkin–Huxley neuronal network. *Communications in Nonlinear Science and Numerical Simulation*, 34, 12–22.

Borges, R. R., Borges, F. S., Lameu, E. L., Batista, A. M., Iarosz, K. C., Caldas, I. L., et al. (2017). Spike timing-dependent plasticity induces non-trivial topology in the brain. *Neural Networks*, 88, 58–64.

Borges, R. R., Borges, F. S., Lameu, E. E., Protachevicz, P. R., Iarosz, K. C., Caldas, I. L., et al. (2017). Synaptic plasticity and spike synchronisation in neuronal networks. *Brazilian Journal of Physics*, 47, 678–688.

Brunel, N. (2000). Dynamics of sparsely connected networks of excitatory and inhibitory spiking neurons. *Journal of Computational Neuroscience*, 8, 183–208.

Brunel, N., & Hakim, V. (1999). Fast global oscillations in networks of integrate-and-fire neurons with low firing rates. *Neural Computation*, *11*, 1621–1671.

Brunel, N., & Hakim, V. (2008). Sparsely synchronized neuronal oscillations. *Chaos*, *18*, 015113.

Brunel, N., & Hansel, D. (2006). How noise affects the synchronization properties of recurrent networks of inhibitory neurons. *Neural Computation*, *18*, 1066–1110.

Brunel, N., & Wang, X.-J. (2003). What determines the frequency of fast network oscillations with irregular neural discharges? I. Synaptic dynamics and excitation-inhibition balance. *Journal of Neurophysiology*, *90*, 415–430.

Buhl, E. H., Tamas, G., & Fisahn, A. (1998). Cholinergic activation and tonic excitation induce persistent gamma oscillations in mouse somatosensory cortex in vitro. *The Journal of Physiology*, *513*, 117–126.

Bullmore, E., & Sporns, O. (2009). Complex brain networks: graph theoretical analysis of structural and functional systems. *Nature Reviews Neuroscience*, *10*, 186–198.

Buzsáki, G. (1986). Hippocampal sharp waves: their origin and significance. *Brain Research*, *398*, 242–252.

Buzsáki, G. (2006). *Rhythms of the brain*. New York: Oxford University Press.

Buzsáki, G., Geisler, C., Henze, D. A., & Wang, X.-J. (2004). Interneuron diversity series: circuit complexity and axon wiring economy of cortical interneurons. *Trends in Neurosciences*, *27*, 186–193.

Buzsáki, G., Urioste, R., Hetke, J., & Wise, K. (1992). High frequency network oscillation in the hippocampus. *Science*, *256*, 1025–1027.

Buzsáki, G., & Wang, X.-J. (2012). Mechanisms of gamma oscillations. *Annual Review of Neuroscience*, *35*, 203–225.

Caporale, N., & Dan, Y. (2008). Spike timing-dependent plasticity: a Hebbian learning rule. *Annual Review of Neuroscience*, *31*, 25–46.

Cardin, J. A. (2012). Dissecting local circuits in vivo: integrated optogenetic and electrophysiology approaches for exploring inhibitory regulation of cortical activity. *Journal de Physiologie (Paris)*, *106*, 104–111.

Castilo, P. E., Chiu, C. Q., & Carroll, R. C. (2011). Long-term synaptic plasticity at inhibitory synapses. *Current Opinion in Neurobiology*, *21*, 328–338.

Chklovskii, D. B., Mel, B. W., & Svoboda, K. (2004). Cortical rewiring and information storage. *Nature*, *431*, 782–788.

Csicsvari, J., Hirase, H., Czurko, A., & Buzsáki, G. (1998). Reliability and statedependence of pyramidal cell-interneuron synapses in the hippocampus: An ensemble approach in the behaving rat. *Neuron*, *21*, 179–189.

Csicsvari, J., Hirase, H., Czurko, A., Mamiya, A., & Buzsáki, G. (1999). Oscillatory coupling of hippocampal pyramidal cells and interneurons in the behaving rat. *The Journal of Neuroscience*, *19*, 274–287.

Dan, Y., & Poo, M.-M. (2004). Spike timing-dependent plasticity of neural circuits. *Neuron*, *44*, 23–30.

Dan, Y., & Poo, M.-M. (2006). Spike timing-dependent plasticity: from synapse to perception. *Physiological Reviews*, *86*, 1033–1048.

Debanne, D., Gähwiler, B. H., & Thompson, S. M. (1998). Long-term synaptic plasticity between pairs of individual CA3 pyramidal cells in rat hippocampal slice cultures. *The Journal of Physiology*, *507*(1), 237–247.

Deisseroth, K., Feng, G., Majewska, A. K., Miesenböck, G., Ting, A., & Schnitzer, M. J. (2006). Next-generation optical technologies for illuminating genetically targeted brain circuits. *The Journal of Neuroscience*, *26*, 10380–10386.

Egger, V., Feldmeyer, D., & Sakmann, B. (1999). Coincidence detection and changes of synaptic efficacy in spiny stellate neurons in rat barrel cortex. *Nature Neuroscience*, *2*, 1098–1105.

Feldman, D. E. (2000). Timing-based LTP and LTD at vertical inputs to layer II/III pyramidal cells in rat barrel cortex. *Neuron*, *27*, 45–56.

Feldman, D. E. (2012). The spike-timing dependence of plasticity. *Neuron*, *75*, 556–571.

Fellous, J., & Sejnowski, T. J. (2000). Cholinergic induction of oscillations in the hippocampal slice in the slow (0.5-2 Hz), theta (5-12 Hz) and gamma (35-70 Hz) bands. *Hippocampus*, *10*, 187–197.

Fino, E., Deniau, J.-M., & Venance, L. (2008). Cell-specific spike-timing-dependent plasticity in GABAergic and cholinergic interneurons in corticostriatal rat brain slices. *Journal Physiology*, *581*, 265–282.

Fino, E., Glowinski, J., & Venance, L. (2005). Bidirectional activity-dependent plasticity at corticostriatal synapses. *The Journal of Neuroscience*, *25*, 11279–11287.

Fisahn, A., Pike, F. G., Buhl, E. H., & Paulsen, O. (1998). Cholinergic induction of network oscillations at 40 hz in the hippocampus in vitro. *Nature*, *394*, 186–189.

Fries, P., Reynolds, J. H., Rorie, A. E., & Desimone, R. (2001). Modulation of oscillatory neuronal synchronization by selective visual attention. *Science*, *291*, 1560–1563.

Froemke, R. C. (2015). Plasticity of cortical excitatory–inhibitory balance. *Annual Review of Neuroscience*, *38*, 195–219.

Froemke, R. C., Tsay, I. A., Raad, M., Long, J. D., & Dan, Y. (2006). Contribution of individual spikes in burst-induced long-term synaptic modification. *Journal of Neurophysiology*, *95*, 1620–1629.

Gaiarsa, J.-L., Caillard, O., & Ben-Ari, Y. (2002). Long-term plasticity at GABAergic and glycinergic synapses: mechanisms and functional significance. *Trends in Neurosciences*, *25*, 564–570.

Garcia-Rill, E. (2015). *Waking and the reticular activating system in health and disease*. London: Elsevier.

Geisler, C., Brunel, N., & Wang, X.-J. (2005). Contributions of intrinsic membrane dynamics to fast network oscillations with irregular neuronal discharges. *Journal of Neurophysiology*, *94*, 4344–4361.

Gerstner, W., Kempter, R., van Hemmen, J. L., & Wagner, H. (1996). A neuronal learning rule for sub-millisecond temporal coding. *Nature*, *383*, 76–81.

Golomb, D., & Rinzel, J. (1994). Clustering in globally coupled inhibitory neurons. *Physica D*, *72*, 259–282.

Gray, C. M. (1994). Synchronous oscillations in neuronal systems: mechanisms and functions. *Journal of Computational Neuroscience*, *1*, 11–38.

Gray, C. M., & Singer, W. (1989). Stimulus-specific neuronal oscillations in orientation columns of cat visual cortex. *Proceedings of the National Academy of Sciences of the United States of America*, *86*, 1698–1702.

Grosse, P., Cassidy, M. J., & Brown, P. (2002). EEG-EMG, MEG-EMG and EMG-EMG frequency analysis: Physiological principles and clinical applications. *Clinical Neurophysiology*, *113*, 1523–1531.

Guare, J. (1990). *Six degrees of separation: A play*. New York: Random House.

Haas, J., Nowotny, T., & Abarbanel, H. D. I. (2006). Spike-timing-dependent plasticity of inhibitory synapses in the entorhinal cortex. *Journal of Neurophysiology*, *96*, 3305–3313.

Hebb, D. O. (1949). *The organization of behavior; a neuropsychological theory*. New York: Wiley & Sons.

Hodgkin, A. L. (1948). The local electric changes associated with repetitive action in a non-medullated axon. *The Journal of Physiology*, *107*, 165–181.

Hong, D.-G., Kim, S.-Y., & Lim, W. (2011). Effect of sparse random connectivity on the stochastic spiking coherence of inhibitory subthreshold neurons. *Journal of the Korean Physical Society*, *59*, 2840–2846.

Izhikevich, E. M. (2000). Neural excitability, spiking and bursting. *International Journal of Bifurcation and Chaos*, *10*, 1171–1266.

Izhikevich, E. M. (2003). Simple model of spiking neurons. *IEEE Transactions on Neural Networks*, *14*, 1569–1572.

Izhikevich, E. M. (2004). Which model to use for cortical spiking neurons? *IEEE Transactions on Neural Networks*, *15*, 1063–1070.

Izhikevich, E. M. (2007). *Dynamical systems in neuroscience*. Cambridge: MIT Press.

Izhikevich, E. M. (2010). Hybrid spiking models. *Philosophical Transactions of the Royal Society A*, *368*, 5061–5070.

Ji, D., & Wilson, M. (2007). Coordinated memory replay in the visual cortex and hippocampus during sleep. *Nature Neuroscience*, *10*, 100–107.

Kaiser, M., & Hilgetag, C. C. (2006). Nonoptimal component placement, but short processing paths, due to long-distance projections in neural systems. *PLoS Computational Biology*, *2*, e95.

Kepecs, A., van Rossum, M. C. W., Song, S., & Tegner, J. (2002). Spike-timing-dependent plasticity: common themes and divergent vistas. *Biological Cybernetics*, *87*, 446–458.

Khodagholy, D., Gelinas, N., & Buzsáki, G. (2017). Learning-enhanced coupling between ripple oscillations in association cortices and hippocampus. *Science*, *358*, 369–372.

Kim, S.-Y., & Lim, W. (2013). Sparsely-synchronized brain rhythm in a small-world neural network. *Journal of the Korean Physical Society*, *63*, 104–113.

Kim, S.-Y., & Lim, W. (2014). Realistic thermodynamic and statistical–mechanical measures for neural synchronization. *Journal of Neuroscience Methods*, *226*, 161–170.

Kim, S.-Y., & Lim, W. (2015a). Effect of small-world connectivity on fast sparsely synchronized cortical rhythms. *Physica A*, *421*, 109–123.

Kim, S.-Y., & Lim, W. (2015b). Fast sparsely synchronized brain rhythms in a scale-free neural network. *Physical Review E*, *92*, 022717.

Kim, S.-Y., & Lim, W. (2018a). Burst synchronization in a scale-free neuronal network with inhibitory spike-timing-dependent plasticity. bioRxiv: https://doi.org/10.1101/321562 (pp. 1–16).

Kim, S.-Y., & Lim, W. (2018b). Effect of spike-timing-dependent plasticity on stochastic burst synchronization in a scale-free neuronal network. *Cognitive Neurodynamics*, *12*, 315–342.

Kim, S.-Y., & Lim, W. (2018c). Stochastic spike synchronization in a small-world neural network with spike-timing-dependent plasticity. *Neural Networks*, *97*, 92–106.

Kornoski, J. (1948). *Conditional reflexes and neuron organization*. Cambridge: Cambridge University Press.

Kullmann, D. M., & Lamsa, K. P. (2007). Long-term synaptic plasticity in hippocampal interneurons. *Nature Reviews Neuroscience*, 8, 687–699.

Kullmann, D. M., Moreau, A. W., Bakiri, Y., & Nicholson, E. (2012). Plasticity of inhibition. *Neuron*, 75, 951–962.

Kwon, O., & Moon, H. T. (2002). Coherence resonance in small-world networks of excitable cells. *Physics Letters A*, 298, 319–324.

Lago-Fernández, L. F., Huerta, R., Corbacho, F., & Sigüenza, J. A. (2000). Fast response and temporal coherent oscillations in small-world networks. *Physical Review Letters*, 84, 2758–2761.

Lamsa, K. P., Kullmann, D. M., & Woodin, M. A. (2010). Spike-timing dependent plasticity in inhibitory circuits. *Frontiers in Synaptic Neuroscience*, 2, 8.

Larimer, P., & Strowbridge, B. W. (2008). Nonrandom local circuits in the dentate gyrus. *The Journal of Neuroscience*, 28, 12212–12223.

Letzkus, J. J., Kampa, B. M., & Stuart, G. J. (2006). Learning rules for spike timing-dependent plasticity depend on dendritic synapse location. *The Journal of Neuroscience*, 26, 10420–10429.

Lim, W., & Kim, S.-Y. (2011). Statistical–mechanical measure of stochastic spiking coherence in a population of inhibitory subthreshold neuron. *Journal of Computational Neuroscience*, 31, 667–677.

Lisman, J., & Spruston, N. (2010). Questions about STDP as a general model of synaptic plasticity. *Frontiers in Synaptic Neuroscience*, 2, 140.

Lizier, J. T., Pritam, S., & Prokopenko, M. (2011). Information dynamics in small-world boolean networks. *Artificial Life*, 17, 293–314.

Logothetis, N. K., Pauls, J., Augath, M. A., Trinath, T., & Oeltermann, A. (2001). Neurophysiological investigation of the basis of the fMRI signal. *Nature*, 412, 150–157.

Longtin, A. (1995). Synchronization of the stochastic Fitzhugh-Nagumo equations to periodic forcing. *Nuovo Cimento D*, 17, 835–846.

Longtin, A. (2000). Stochastic aspects of neural phase locking to periodic signals. In S. Kim, K. J. Lee, & W. Sung (Eds.), *Stochastic dynamics and pattern formation in biological and complex systems* (pp. 219–239). New York: AIP.

Lourens, M. A. J., Schwab, B. C., Nirody, J. A., Meijer, H. G. E., & van Gils, S. A. (2015). Exploiting pallidal plasticity for stimulation in Parkinson's disease. *Journal of Neural Engineering*, 12, 026005.

Markram, H., Gerstner, W., & Sjöström, P. J. (2011). A history of spike-timing-dependent plasticity. *Frontiers in Synaptic Neuroscience*, 3, 4.

Markram, H., Gerstner, W., & Sjöström, P. J. (2012). Spike-timing-dependent plasticity: a comprehensive overview. *Frontiers in Synaptic Neuroscience*, 4, 2.

Markram, H., Lübke, J., Frotscher, M., & Sakmann, B. (1997). Regulation of synaptic efficacy by coincidence of postsynaptic APs and EPSPs. *Science*, 275, 213–215.

Mehta, M. R., & Wilson, M. (2000). From hippocampus to V1: Effect of LTP on spatiotemporal dynamics of receptive fields. *Neurocomputing*, 32, 905–911.

Michalareas, G., Vezoli, J., van Pelt, S., Schoffelen, J. M., Kennedy, H., & Fries, P. (2016). Alpha-beta and gamma rhythms subserve feedback and feedforward influences among human cortical areas. *Neuron*, 89, 384–397.

Milgram, S. (1967). The small-world problem. *Psychology Today*, 1, 61–67.

Miyawaki, H., & Diva, K. (2016). Regulation of hippocampal firing by network oscillations during sleep. *Current Biology*, 26, 893–902.

Morrison, A., Aertsen, A., & Diesmann, M. (2007). Spike-timing dependent plasticity in balanced random networks. *Neural Computation*, 19, 1437–1467.

Morrison, A., Diesmann, M., & Gerstner, W. (2008). Phenomenological models of synaptic plasticity based on spike timing. *Biological Cybernetics*, 98, 459–478.

olde Scheper, T. V., Meredith, R. M., Mansvelder, H. D., van Pelt, J., & van Ooyen, A. (2018). Dynamic Hebbian cross-correlation learning resolves the spike timing dependent plasticity conundrum. *Frontiers in Computational Neuroscience*, 11, 119.

Oliva, A., Fernández-Ruiz, A., Buzsáki, G., & Berényi, A. (2016). Role of hippocampal CA2 region in triggering sharp-wave ripples. *Neuron*, 91, 1–14.

Ozer, M., Perc, M., & Uzuntarla, M. (2009). Stochastic resonance on Newman-Watts networks of Hodgkin–Huxley neurons with local periodic driving. *Physics Letters A*, 373, 964–968.

Pfister, J.-P., & Gerstner, W. (2006). Triplets of spikes in a model of spike timing-dependent plasticity. *The Journal of Neuroscience*, 26, 9673–9682.

Ploner, M., Sorg, C., & Gross, J. (2017). Brain rhythms of pain. *Trends in Cognitive Sciences*, 21, 100–110.

Popovych, O. V., & Tass, P. A. (2012). Desynchronizing electrical and sensory coordinated reset neuromodulation. *Frontiers in Human Neuroscience*, 6, 58.

Popovych, O. V., Yanchuk, S., & Tass, P. A. (2013). Self-organized noise resistance of oscillatory neural networks with spike-timing-dependent plasticity. *Scientific Reports*, 3, 2926.

Riecke, H., Roxin, A., Madruga, S., & Solla, S. (2007). Multiple attractors, long chaotic transients, and failure in small-world networks of excitable neurons. *Chaos*, 17, 026110.

Roux, L., Hu, B., Eichler, R., Stark, E., & Buzsáki, G. (2017). Sharp wave ripples during learning stabilize the hioppocampal map. *Nature Neuroscience*, 20, 845–853.

Roxin, A., Riecke, H., & Solla, S. A. (2004). Self-sustained activity in a small-world network of excitable neurons. *Physical Review Letters*, 92, 198101.

Rubin, J., Lee, D. D., & Sompolinsky, H. (2001). Equilibrium properties of temporally asymmetric Hebbian plasticity. *Physical Review Letters*, 86, 364–367.

Saleem, A. B., Lien, A. D., Krumin, M., Haider, B., Rosón, M. R., Ayaz, A., et al. (2017). Subcortical source and modulation of the narrowband gamma oscillation in mouse visual cortex. *Neuron*, 93, 315–322.

San Miguel, M., & Toral, R. (2000). Stochastic effects in physical systems. In J. Martinez, R. Tiemann, & E. Tirapegui (Eds.), *Instabilities and nonequilibrium structures VI* (pp. 35–130). Dordrecht: Kluwer Academic Publisher.

Sejnowski, T. J. (1977). Storing covariance with nonlinearly interacting neurons. *Journal of Mathematical Biology*, 4, 303–321.

Shanahan, M. (2008). Dynamical complexity in small-world networks of spiking neurons. *Physical Review E*, 78, 041924.

Shatz, C. J. (1992). The developing brain. *Scientific American*, 267, 60–67.

Shimazaki, H., & Shinomoto, S. (2010). Kernel bandwidth optimization in spike rate estimation. *Journal of Computational Neuroscience*, 29, 171–182.

Shin, S. L., & De Schutter, E. (2006). Dynamic synchronization of Purkinje cell simple spikes. *Journal of Neurophysiology*, 96, 3485–3491.

Singer, W. (1999). Neuronal synchrony: a versatile code for the definition of relations? *Neuron*, 24, 49–65.

Singer, W., & Gray, C. (1995). Visual feature integration and the temporal correlation hypothesis. *Annual Reviews Neuroscience*, 18, 555–586.

Sjöström, P. J., & Häusser, M. (2006). A cooperative switch determines the sign of synaptic plasticity in distal dendrites of neocortical pyramidal neurons. *Neuron*, 51, 227–238.

Song, S., & Abbott, L. F. (2001). Cortical development and remapping through spike timing-dependent plasticity. *Neuron*, 32, 339–350.

Song, S., Miller, K. D., & Abbott, L. F. (2000). Competitive Hebbian learning through spike-timing-dependent plasticity synaptic plasticity. *Nature Neuroscience*, 3, 919–926.

Song, S., Sjöström, P. J., Reigl, M., Nelson, S., & Chklovskii, D. B. (2005). Highly nonrandom features of synaptic connectivity in local cortical circuits. *PLoS Biology*, 3, e68.

Soto-Trevino, C., Thoroughman, K. A., Marder, E., & Abbott, L. F. (2001). Activity-dependent modification of inhibitory synapses in models of rhythmic neural networks. *Nature Neuroscience*, 4, 297–303.

Sporns, O. (2011). *Networks of the brain*. Cambridge: MIT Press.

Sporns, O., & Honey, C. J. (2006). Small worlds inside big brains. *Proceedings of the National Academy of Sciences of the United States of America*, 103, 19219–19220.

Sporns, O., Tononi, G., & Edelman, G. M. (2000). Theoretical neuroanatomy: relating anatomical and functional connectivity in graphs and cortical connection matrices. *Cerebral Cortex*, 10, 127–141.

Stent, G. S. (1973). A physiological mechanism for Hebb's postulate of learning. *Proceedings of the National Academy of Sciences of the United States of America*, 70, 997–1001.

Strogatz, S. H. (2001). Exploring complex networks. *Nature*, 410, 268–276.

Swann, N. C., de Hemptinne, C., Miocinovic, S., Qasim, S., Wang, S. S., Ziman, N., et al. (2017). Gamma oscillations in the hyperkinetic state detected with chronic human brain recordings in Parkinson's disease. *The Journal of Neuroscience*, 36, 6445–6458.

Talathi, S. S., Hwang, D. U., & Ditto, W. L. (2008). Spike timing dependent plasticity promotes synchrony of inhibitory networks in the presence of heterogeneity. *Journal of Computational Neuroscience*, 25, 262–281.

Tass, P., Rosenblum, M. G., Weule, J., Kurths, J., Pikovsky, A., Volkmann, J., et al. (1998). Detection of $n : m$ phase locking from noisy data: application to magnetoencephalography. *Physical Review Letters*, 81, 3291–3294.

Taxidis, J., Anastassiou, C. A., Diva, K., & Koch, C. (2015). Local field potentials encode place cell ensemble activation during hippocampal sharp wave ripples. *Neuron*, 87, 590–604.

Traub, R. D., & Whittington, M. A. (2010). *Cortical oscillations in health and diseases*. New York: Oxford University Press.

Tzounopoulos, T., Kim, Y., Oertel, D., & Trussell, L. O. (2004). Cell-specific, spike timing-dependent plasticities in the dorsal cochlear nucleus. *Nature Neuroscience*, 7, 719–725.

Uhlhaas, P., & Singer, W. (2006). Neural synchrony in brain disorders: relevance for cognitive dysfunctions and pathophysiology. *Neuron*, 52, 155–168.

Uhlhaas, P., & Singer, W. (2010). Abnormal neural oscillations and synchrony in schizophrenia. *Nature Reviews Neuroscience*, *11*, 100–113.

Ujma, P. P., Bódizs, R., Gombos, F., Stintzing, J., Konrad, B. N., Ginzel, L., et al. (2015). Nap sleep spindle correlates of intelligence. *Scientific Reports*, *5*, 17159.

Veit, J., Hakim, R., Jadi, M. P., Sejnowski, T. J., & Adesnik, H. (2017). Cortical gamma band synchronization through somatostatin interneurons. *Nature Neuroscience*, *20*, 951–959.

Vogels, T. P., Froemke, R. C., Doyon, N., Gilson, M., Haas, J. S., Liu, R., et al. (2013). Inhibitory synaptic plasticity: spike timing-dependence and putative network function. *Frontiers in Neural Circuits*, *7*, 119.

Vogels, T. P., Sprekeler, H., Zenke, F., Clopath, C., & Gerstner, W. (2011). Inhibitory plasticity balances excitation and inhibition in sensory pathways and memory networks. *Science*, *334*, 1569–1573.

von der Malsburg, C. (1973). Self-organization of orientation sensitive cells in the striate cortex. *Kybernetik*, *14*, 85–100.

Wang, X.-J. (2003). Neural oscillations. In L. Nadel (Ed.), *Encyclopedia of cognitive science* (pp. 272–280). London: MacMillan.

Wang, X.-J. (2010). Neurophysiological and computational principles of fscortical rhythms in cognition. *Physiological Reviews*, *90*, 1195–1268.

Wang, X.-J., & Buzsáki, G. (1996). Gamma oscillations by synaptic inhibition in a hippocampal interneuronal network. *The Journal of Neuroscience*, *16*, 6402–6413.

Wang, Q., Duan, Z., Perc, M., & Chen, G. (2008). Synchronization transitions on small-world neuronal networks: Effects of information transmission delay and rewiring probability. *EPL*, *83*, 50008.

Wang, Q., Perc, M., Duan, Z., & Chen, G. (2010). Impact of delays and rewiring on the dynamics of small-world neuronal networks with two types of coupling. *Physica A*, *389*, 3299–3306.

Watts, D. J. (2003). *Small worlds: The dynamics of networks between order and randomness*. Princeton University Press.

Watts, D. J., & Strogatz, S. H. (1998). Collective dynamics of 'small-world' networks. *Nature*, *393*, 440–442.

Whittington, M. A., Traub, R. D., Kopell, N., Ermentrout, B., & Buhl, E. H. (2000). Inhibition-based rhythms: experimental and mathematical observations on network dynamics. *International Journal of Psychophysiology*, *38*, 315–336.

Wittenberg, G. M., & Wang, S. S. (2006). Malleability of spike-timing-dependent plasticity at the CA3-CA1 synapse. *The Journal of Neuroscience*, *26*, 6610–6617.

Woodin, M. A., Ganguly, K., & Poo, M.-M. (2003). Coincident pre- and postsynaptic activity modifies GABAergic synapses by postsynaptic changes in Cl- transporter activity. *Neuron*, *39*, 807–820.

Yu, S., Huang, D., Singer, W., & Nikolie, D. (2008). A small world of neuronal synchrony. *Cerebral Cortex*, *18*, 2891–2901.

Zhang, L. I., Tao, H. W., Holt, C. E., Harris, W. A., & Poo, M. (1998). A critical window for cooperation and competition among developing retinorectal synapses. *Nature*, *395*, 37–44.